PERSPECTIVES IN FLUID DYNAMICS

A Collective Introduction to Current Research

Edited by

G. K. Batchelor

H. K. Moffatt

M. G. Worster

CAMBRIDGE
UNIVERSITY PRESS

2

Viscous Fingering as an Archetype for Growth Patterns

YVES COUDER

1 Introduction

Perhaps because man has had to survive in the wild for so long, our eye (or rather our brain) is extremely well trained in detecting and recognizing patterns. We also have a spontaneous tendency to relate them to each other. When describing sand dunes we compare them to sea waves. When speaking of ice crystals we use a vocabulary, e.g. dendrites, branches etc., borrowed from botany. The book *On Growth and Form* by D'Arcy Thompson (1917) was the first written attempt to list such analogies and seek their possible underlying physical bases. For this reason it has become an essential reference in the field of morphogenesis – the appearance and evolution of shape.

In a wide variety of situations the formation of patterns results from a growth process. Growth gives form to living entities but also generates patterns by a variety of physical processes. Such processes include viscous fingering, dendritic growth of crystals, electrodeposition, growth of bacterial colonies, propagation of flame fronts, fractures in brittle solids, dielectric breakdown, diffusion-limited aggregation, corrosion of solids, etc. All these problems belong to a class often called free-boundary problems.

These phenomena have been investigated for fundamental reasons but also because of the needs of industrial research. From this point of view the morphogenetic instabilities are often considered a nuisance and studied to find ways to avoid their occurrence. For instance the petroleum industry has been consistently trying to find ways of inhibiting viscous fingering because it limits oil recovery in porous media (see § 2.4). Viscous instabilities are also a limitation in coating processes where a fluid has to be spread evenly onto a solid surface (see § 6). Similarly, engineers seeking to obtain a good metal plating try to avoid any fractal or dendritic growth in electrodeposition. These instabilities can also be beneficial: the intricacies of the dendrites in

the solidification of steel are essential for its mechanical properties. Fractal growth, because it builds up structures with a large interface, can be used to improve catalytic effects and is vital for the formation of our lungs for instance.

During the last twenty years the investigation of a hydrodynamic instability discovered by Saffman & Taylor in 1958 has served as a reference in the field of pattern formation. It has the advantage of being experimentally simple. The theory, complex as it may seem, still provides the best understanding of a pattern-forming system. Saffman–Taylor fingering is thus studied for reasons which go beyond its pure hydrodynamic interest, and will be the guiding theme of this chapter.

Another pattern-forming phenomenon is solidification. Although the two fields of research – viscous fingering and solidification – developed independently (at least initially), there is a remarkable parallel between the successive steps of research in the two areas. The linear stability analysis of a plane front was published for viscous fingering by Chuoke, Van Meurs & Van der Pol in 1959 and for solidification by Mullins & Sekerka in 1964. The existence (in the absence of surface tension) of families of solutions having the shape of curved fronts was demonstrated by Saffman & Taylor (1958) for viscous fingers. It had been preceded by a similar demonstration, by Ivantsov (1947), for parabolic needle crystals. The selection of the observed solutions was understood much later, at a time when everyone had become aware of the similarities between the two problems. Both were solved progressively in the 1980s by the converging efforts of many researchers.

Early reviews on the development of this area are in Saffman (1986), Bensimon *et al.* (1986) and Homsy (1987). More recent ones, presented from a variety of viewpoints, are in Pelcé (1988), Kessler, Koplik & Levine (1988), Couder (1991), Tanveer (1991), Pomeau & Ben Amar (1992) and McCloud & Maher (1995).

1.1 Growth in a Laplacian field

The best way to find out what viscous fingers look like is to do an experiment. Take two circular glass plates, one of them having a central injection hole. Set the plates horizontally, clamped together but separated by thin spacers (of typical thickness 0.3 mm). First fill the cell with a viscous fluid, e.g. silicon oil, then blow air into the central hole so as to push the oil out radially. An example of what you will see is given in figure 1. The air does not penetrate the oil regularly to form a circular region but forms a pattern which becomes increasingly complex. This experiment is the axisymmetric variant

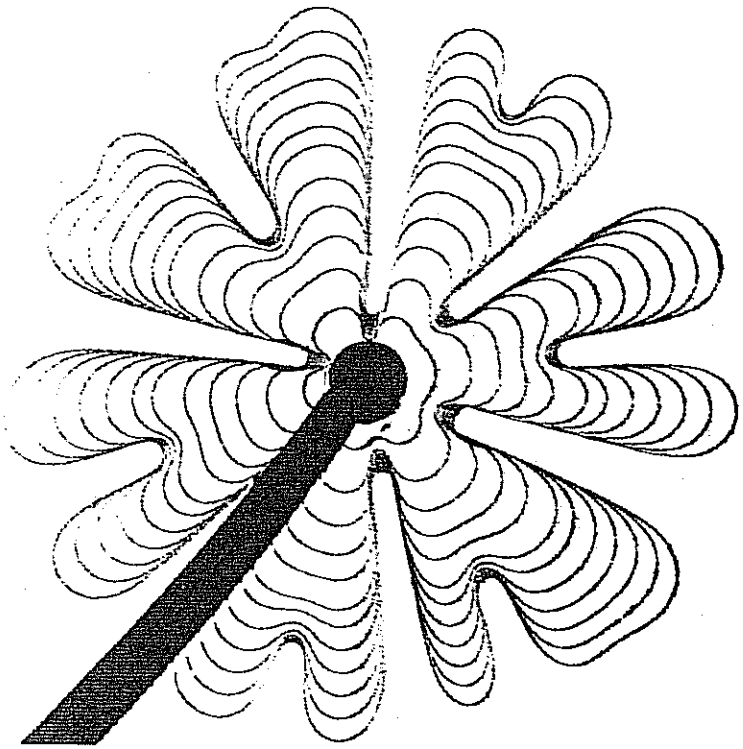

Figure 1. A superposition of successive states of a radial Saffman–Taylor pattern.

of viscous fingering introduced by Bataille (1968) and by Paterson (1981). In this instability, the two fluids and their interface move due to the applied pressure. As shown below (see §2.1) the fluids have a Poiseuille flow driven by the applied pressure. The experimental situation can thus be described by a two-dimensional model where the spatial distribution of pressure forms a Laplacian field and the fluids move with a velocity proportional to the gradients of pressure. Thus schematized, this experiment is reduced to a general problem sometimes called the inverse Stefan problem. It turns out that other morphogenetic systems, such as for instance diffusion-limited aggregation (see §3.1), can be reduced to the same mathematical problem. The mathematical ingredients for this type of growth are the following.

An interface (figure 2) separates two regions of a plane respectively labelled (1) and (2). There exists a scalar field $P(x, y, t)$ in this plane. In the case of Saffman–Taylor fingering this field P is the pressure p. In the simplest cases P is constant in region 1 and in region 2 satisfies the Laplacian:

$$\nabla^2 P = 0. \tag{1.1}$$

At a given time, the determination of the field P depends on the boundary conditions defined at infinity and at the interface between regions 1 and 2. We are interested in situations in which this interface moves in the local gradient of P with a normal velocity

$$V_n \propto \boldsymbol{n} \cdot \nabla P, \tag{1.2}$$

where $\boldsymbol{n}$ is the unit vector normal to the interface. The displacement of the interface, because it changes the location of a boundary, modifies the field P and thus, in turn, the interface velocity. This process leads to an instability which generates a pattern. The whole process is strongly non-local, due to the long-range interactions introduced by Laplace's law.

Two remarks can be made

(i) These dynamical equations are also obtained for other processes. As we will see in § 3.1, the growth in diffusion-limited aggregation (DLA) is also described by equations (1.1) and (1.2) where P is a different type of quantity (a probability density). In both Saffman–Taylor fingering and DLA the dynamics defined by these equations results in the spontaneous formation of a ramified pattern where the growth occurs essentially at the protruding extremities.

(ii) It can be noted that equations (1.1) and (1.2) are mathematically the fundamental equations of electrostatics. In this analogy, *at a given time* the velocity corresponds to the electric field and P to the electric potential. Though in the present case these equations are dynamical we shall use this analogy to obtain an intuitive understanding of the origin of the instability.

Returning to the Saffman–Taylor problem we consider (figure 2) a situation where the two fluids are initially separated by a flat interface and we assume this interface to be disturbed by a small protrusion of typical size L. The curves of constant values of P will be parallel lines, only distorted in front of the bump. It is a property of Laplacian fields that this distortion will only affect these curves to a "depth" of the order of L. As a result the gradient of P is locally larger in front of the protrusion (see figure 2) and so is the velocity. The amplitude of the protrusion will thus grow: the interface is unstable. This amplification of the velocity is equivalent to the amplification of the electric field by the point effect in electrostatics. Note that if the fluids were moving in the opposite direction, i.e. if the more-viscous fluid was forcing the less-viscous one to recede, the change in velocity would serve to reduce the protrusion and the front would be stable.

Ideally, in the absence of any other factor, the more pointed the protrusion

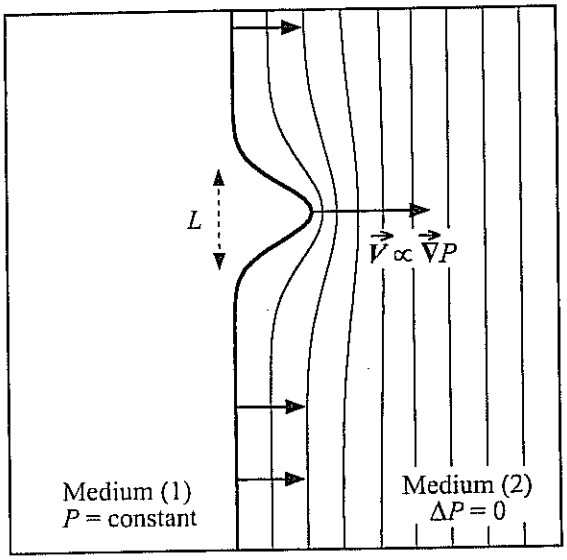

Figure 2. Sketch of the lines of constant values of the scalar field P in front of a local disturbance of a plane front (in the absence of surface tension).

the larger the gradient and the velocity. For this reason several works have suggested that in this case the instability will lead to the formation of cusp-like singularities in finite time (Shraiman & Bensimon 1984; Howison 1986; Bensimon & Pelcé 1986). However, in real experiments, additional effects due to the interfacial capillarity effect are present which stabilize the interface at small scales.

In order to account quantitatively for the various effects, it is necessary to perform a linear stability analysis (as done for Saffman–Taylor fingering in §2). The validity of the linear stability analysis is, in principle, limited to small-amplitude perturbations. In reality it provides a length scale which retains its validity for large-amplitude fingers. As the protrusions continue growing they interact non-locally. Two situations can eventually be reached: steady curved fronts can be obtained when the system is confined (§4) or fractal structures build up when it is not (§5). For both types of growth three factors are determinant: the length scales of the problem; the geometry of the cell; the isotropy or the non-isotropy of the system.

1.2 Growth in a diffusive field

In a related family of problems the field P is diffusive and equation (1.1) is replaced by

$$\frac{\partial P}{\partial t} = D\nabla^2 P, \tag{1.3}$$

while equation (1.2) remains the same. In solidification for instance, the growth is linked to either the diffusion of heat or that of impurities (see chapter 8). Similarly, the growth in bacterial colonies is limited by the diffusion of a nutrient in a gel. The front is unstable and the previous intuitive argument (figure 2) can be used again here. However, at large amplitudes, the interaction of different structures is different from the Laplacian case. With a diffusive field the thickness of the disturbed region in the vicinity of an interface moving at velocity V is bounded by the diffusion length $l_D = D/V$. Regions of the interface separated from each other by more than l_D will behave independently. For this reason l_D will be a lower limit to the scales on which the pattern can have a fractal structure. Only at very small velocities will l_D be very large and the behaviour of the system close to what it would be with a Laplacian field.

1.3 Directional growth

Finally, in a third type of situation, the experimental set-up is designed so as to impose a fixed gradient on the scalar P. The mean direction of the growth is then fixed by the orientation of this gradient. The archetype of such growth is the directional growth of crystals where the solidification front is confined by an imposed mean temperature gradient. There is also a directional type of viscous fingering in which a pressure gradient is imposed. In general, the system, being stabilised at small scales by the capillary effects and at large scales by the gradient, can have a stable plane front at low velocities. Beyond a finite threshold it destabilizes into a cellular pattern having a periodicity predicted by the linear stability analysis. The further evolution of the pattern is completely different from that of free growth. The gradient generates stabilizing nonlinear terms so that the amplitude of the cells saturates. These systems are one-dimensional and are investigated for two reasons. From a practical point of view they are of interest to the coating industry, because this instability imposes a limit on the velocity at which it is possible to spread a fluid onto a solid. From a fundamental point of view they serve as archetypes of the dynamics of one-dimensional spatially extended dynamical systems. They exhibit spatio–temporal chaos, propagating waves, solitary waves and other nonlinear processes. A few of their characteristics will be presented in § 6.

2 The basis of Saffman–Taylor viscous fingering instability

2.1 Potential flow in a Hele-Shaw cell

We first consider a single fluid flowing in a Hele-Shaw cell formed by two parallel plates separated by a narrow gap of thickness b. The frame of

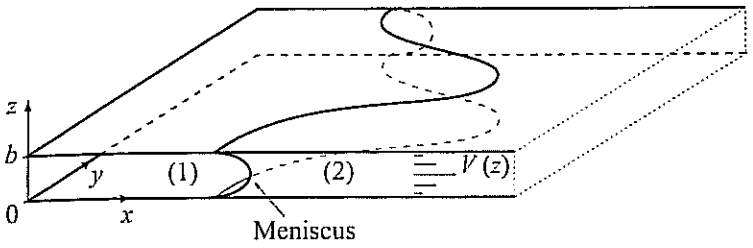

Figure 3. Sketch of the Hele-Shaw cell.

reference is given in figure 3. The motion is driven by pressure and limited by viscous friction so that the Navier–Stokes equation reduces to

$$\nabla p = \mu \nabla^2 \boldsymbol{u}. \tag{2.1}$$

Since the thickness is small, only the velocity components parallel to the plates are considered. Their dominant variation is in the z-direction so that (2.1) can be written

$$\nabla p = \mu \frac{\partial^2 \boldsymbol{u}}{\partial z^2}, \tag{2.2}$$

which can be integrated to give the parabolic velocity field of plane Poiseuille flow:

$$\boldsymbol{u} = \frac{1}{2\mu} z(z - b)\nabla p. \tag{2.3}$$

Integrating the flow through the cell thickness, we define an average velocity $\langle \boldsymbol{u} \rangle$ by

$$\boldsymbol{Q} = \int_0^b \boldsymbol{u} \mathrm{d}z = \langle \boldsymbol{u} \rangle b \tag{2.4}$$

and find that $\langle \boldsymbol{u} \rangle$ is governed by the potential law

$$\langle \boldsymbol{u} \rangle = -\frac{b^2}{12\mu} \nabla p. \tag{2.5}$$

This relation between mean velocity and pressure is a particular case of Darcy's law, which holds more generally for fluids moving through porous media such as e.g. rocks or piles of glass beads. It is usually written

$$\langle \boldsymbol{u} \rangle = -K \nabla p, \tag{2.6}$$

where K is the permeability of the medium.

Finally, in both a Hele-Shaw cell and in a porous medium, since the fluid is incompressible, $\nabla \cdot \langle \boldsymbol{u} \rangle = 0$ and the pressure is a Laplacian field,

$$\nabla^2 p = 0. \tag{2.7}$$

In the following we will adopt the two-dimensional approximation where the velocities of the fluid are the average ones satisfying relation (2.6) and we will omit the average symbol.

2.2 Linear stability analysis of the front between two fluids of different viscosity

The Saffman–Taylor instability occurs in a Hele-Shaw cell at the interface between two fluids of different viscosities when the fluid of low viscosity displaces the fluid of higher viscosity. In order to neglect the possible effect of the difference of density, we will suppose the cell to be horizontal. The flow of each fluid satisfies relation (2.5) so that

$$\boldsymbol{u}_i = K_i \nabla p_i \tag{2.8}$$

where $i = 1$ or 2 respectively for the two fluids and where

$$K_i = -\frac{b^2}{12\mu_i}. \tag{2.9}$$

The pressure distribution on the two sides of the interface satisfies

$$\nabla^2 p_i = 0. \tag{2.10}$$

The linear stability analysis is used to predict whether a flow is stable. In the case of a spatially extended system this analysis has to be performed with regard to perturbations of all spatial periodicities. For this purpose we apply to a straight interface a periodic disturbance of arbitrary wave-vector $\boldsymbol{k}$. We then compute, in a linear approximation, whether this disturbance will grow. For viscous fingering this linear analysis was first performed by Chuoke *et al.* (1959).

2.2.1 The basic flow

The Hele-Shaw cell is represented by an infinite plane in which the two different fluids occupy two half-planes separated by a linear interface (dashed line on figure 4). In the basic state the two fluids move with the same average velocity V along the x-axis:

$$u_i^0 = V. \tag{2.11}$$

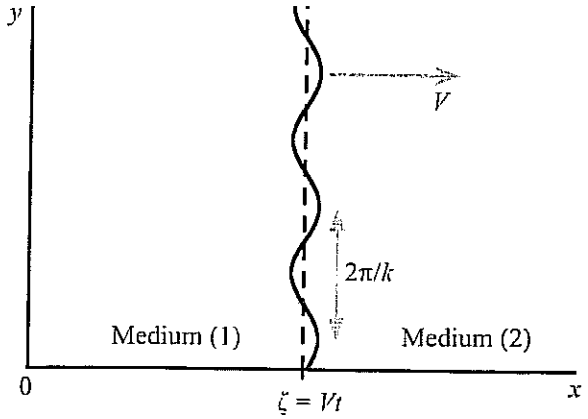

Figure 4. Definition of the axes for the stability analysis. For Chuoke's analysis of viscous fingering the front separates fluid (1) on the left from fluid (2). For solidification (§ 3.2) (1) is the solid, (2) is the liquid.

The pressure distribution is found by integrating (2.8) and choosing the pressure to be zero on the interface located at $x = \zeta = Vt$,

$$p_i^0 = \frac{V}{K_i}(x - Vt). \tag{2.12}$$

2.2.2 The disturbance of the interface

A sinusoidal disturbance of wave-vector k is then imposed on the interface (figure 4). The aim of our calculation will be to find whether the amplitude of the disturbance will grow in time (unstable situation) or decrease in time (stable situation). The amplitude of the disturbance is thus chosen as $\epsilon\exp(\sigma t)$ where ϵ is small. Should σ be negative for all k the front will be stable. If it is positive for a range of values of k the flow will be unstable for perturbations having these wave-vectors. The interface at time t is now given by

$$\zeta = Vt + \epsilon e^{\sigma t}\sin ky. \tag{2.13}$$

The velocity field and the pressure field are disturbed and can be written as

$$p_i^T = p_i^0 + p_i, \qquad \boldsymbol{u}_i^T = \boldsymbol{u}_i^0 + \boldsymbol{u}_i. \tag{2.14}$$

Darcy's law (equation (2.8)) and the incompressibility constraint (2.10) are valid for both the undisturbed fields ($\boldsymbol{u}_i^0$ and p_i^0) and the total disturbed field ($\boldsymbol{u}_i^T$ and p_i^T). They thus also hold for the disturbance ($\boldsymbol{u}_i$ and p_i). Using them we can compute the correction to the pressure distribution. We seek

solutions of the form

$$p_i = p_i'(x,t)\sin ky \tag{2.15}$$

having the same spatial periodicity. The amplitude p_i' must grow or decrease in time with the interface disturbance itself. Its dependence on x must be such that on moving away from the interface the disturbance of the pressure field decreases to zero. As the pressure is a Laplacian field (2.10) it must decrease exponentially with a length scale fixed by the wavelength of the disturbance. So we must have

$$p_1 = A_1 e^{\sigma t + kx}\sin ky, \qquad p_2 = A_2 e^{\sigma t - kx}\sin ky. \tag{2.16}$$

2.2.3 Continuity of the normal velocities at the interfaces

The continuity of the normal components of the velocity at the interface,

$$u_{n_1} = u_{n_2}, \tag{2.17}$$

can be approximated, in the limit of small deformations, by the continuity of the velocities along Ox

$$u_{x_1} = u_{x_2} = \frac{\partial \zeta}{\partial t} - V, \tag{2.18}$$

so that

$$K_i \left(\frac{\partial p_i}{\partial x}\right)_{x=\zeta} = \epsilon\sigma e^{\sigma t}\sin ky. \tag{2.19}$$

Using (2.16) and keeping only the first-order terms by taking $\zeta = Vt$ we thus determine A_1 and A_2. The pressure on each side is now given by

$$p_1 = \frac{\epsilon\sigma}{K_1 k} e^{\sigma t + k(x - Vt)}\sin ky, \qquad p_2 = -\frac{\epsilon\sigma}{K_2 k} e^{\sigma t - k(x - Vt)}\sin ky. \tag{2.20}$$

2.2.4 The pressure jump at the interface due to surface tension

The problem is completed by the interfacial effects due to capillarity. They create a pressure jump Δp given by Laplace's law between the two sides of a curved interface,

$$\Delta p = \gamma(\kappa_1 + \kappa_2), \tag{2.21}$$

where γ is the surface tension and κ_1 and κ_2 are the two main curvatures of the interface. In the most common Saffman–Taylor experimental situation, a gas forces oil into motion; the oil wets the solid walls so that the two fluids are separated by a meniscus as sketched in figure 3. The strongest curvature of the interface is perpendicular to the plane of the cell. But the analysis of the Saffman–Taylor instability is two-dimensional. The curvature

κ_2 is thus considered to be of the order of $\kappa_2 \approx 2/b$ and constant along the interface, so that its dynamical effect can be neglected. Only κ_1 is taken into account. This is a bold assumption as it neglects the fact that when the viscous fluid is pushed out of the cell it leaves on the solid surfaces two wetting films having a thickness which is a function of the normal velocity of the interface (Landau & Levich 1942; Bretherton 1961). This assumption is not always valid as has been shown experimentally (Tabeling, Zocchi & Libchaber 1987) and theoretically (Reinelt 1987). Tanveer (1990) has treated the complete three-dimensional system and shown within which limits the two-dimensional assumption is valid.

Returning to the two-dimensional stability analysis and neglecting the higher order terms in the expression for the curvature, we can write,

$$p_2^T(\zeta) - p_1^T(\zeta) = \gamma \frac{\partial^2 \zeta}{\partial y^2}, \tag{2.22}$$

where

$$p_2^T(\zeta) - p_1^T(\zeta) = p_2^0(\zeta) - p_1^0(\zeta) + p_2(\zeta) - p_1(\zeta). \tag{2.23}$$

We use equations (2.12) and (2.20) for the different pressures. In order to retain only the first-order terms we take ζ equal to Vt in the last two terms $(p_2(\zeta) - p_1(\zeta))$. After a simple calculation we obtain an expression for the amplification rate:

$$\sigma = \left(\frac{K_1 - K_2}{K_1 + K_2}\right) Vk + \gamma \left(\frac{K_1 K_2}{K_1 + K_2}\right) k^3 \tag{2.24}$$

or, returning to the physical variables,

$$\sigma = \left(\frac{\mu_2 - \mu_1}{\mu_1 + \mu_2}\right) Vk - \gamma \frac{b^2}{12} \left(\frac{1}{\mu_1 + \mu_2}\right) k^3. \tag{2.25}$$

In the case of a gas displacing a high-viscosity fluid such as oil, $\mu_2 \gg \mu_1$, so that taking $\mu_1 = 0$ and $\mu_2 = \mu$, equation (2.25) simplifies to:

$$\sigma = Vk - \gamma \frac{b^2}{12\mu} k^3. \tag{2.26}$$

Figure 5 shows a graph of $\sigma(k)$ for two values of V in the case where $\mu_2 > \mu_1$. For a given velocity V the disturbance of maximum growth rate σ has a wave-vector

$$k_c = \frac{2}{b}\sqrt{\frac{\mu V}{\gamma}}, \tag{2.27}$$

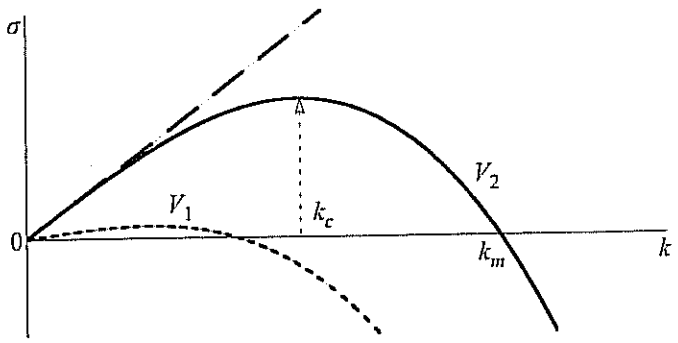

Figure 5. The wave-vector dependence of the amplification rate predicted by the linear analysis of viscous fingering due to Chuoke *et al.* (1959) (equation (2.26)). A similar result is found in the analysis by Mullins & Sekerka (1964) of a solidification front (equation (3.7)).

corresponding to the most unstable wavelength

$$l_c = \pi b \sqrt{\frac{\gamma}{\mu V}}, \tag{2.28}$$

usually called the capillary length of the instability. The interface is unstable to all perturbations of wave-vectors smaller than $k_{\max} = \sqrt{3}k_c$. For all positive velocities there is a range of k for which $\sigma > 0$: when the fluid of smaller viscosity forces the fluid of larger viscosity to recede, the interface is always unstable. In the reverse situation (i.e. when $V < 0$), σ is negative for all k and the interface is stable.

2.3 Miscible fluids

As demonstrated by the linear stability analysis the existence of the limiting small scale l_c results from the capillary forces at the interface between two immiscible fluids. What happens in the absence of surface tension? To answer this question experiments have been performed using two miscible fluids (e.g. water and glycerol). In this case there is still formation of fingers but they have a fixed scale of the order of $3b$, where (b is the cell's thickness). This means that the system spontaneously locks onto a new small scale but the flow has become fully three-dimensional. None of the hypotheses on which the above stability calculations are based can be used in this case (Paterson 1985).

2.4 Fingering in porous media

A very similar type of instability occurs in porous media, which is of great importance during oil recovery in oil fields (see Po Zen Wong 1999 and references therein). Usually, immediately after the drilling of a new well, oil flows out of it spontaneously. However when this spontaneous process stops most of the oil is still locked in the deposit as it is absorbed in porous rocks. If several wells are drilled near to each other it is possible then to force the oil to flow out of one of them by injecting high pressure water in the others. Unfortunately the flow of the two fluids in the porous medium satisfies equations (1.1) and (1.2) and water is less viscous than oil. As a result the front is unstable and fingers of water will rapidly reach the extraction well and short circuit the motion of the oil. Various tricks with additives in the water are used to try to avoid this situation. Even though Saffman–Taylor fingering can be used here as a model, the natural situation is more complex because of the variable permeability of the rocks and of the role of wetting.

3 The basis of the instability of other physical systems

3.1 Diffusion-limited aggregation

The aggregation of particles limited by diffusion is a physical process (observed in soot for example) which inspired a frequently investigated numerical model system introduced by Witten & Sander (1981, 1983). In a plane system, particles are created, one at a time, far away from a central seed. They perform a random walk on the underlying square lattice. If a particle visits any of the sites neighbouring the central seed, it remains there. The process is repeated a large number of times, each particle sticking whenever it visits a site neighbouring a site already occupied. The growth is therefore radial and results in a fractal aggregate, which has been frequently investigated. In a variant of this model particles come from far away to stick to a linear baseline. Figure 6 shows a fractal DLA resulting from such a simulation. The similarity of DLA with viscous fingering was pointed out by Paterson (1984). The scalar field is here the probability P_v of visit by a randomly walking particle to a given lattice site. With a steady flux of particles from a source far away it obeys a Laplacian law

$$\nabla^2 P_v = 0. \tag{3.1}$$

The average speed at which a region of the aggregate grows is proportional to the local gradient of P_v

$$V_n = \nabla P_v. \tag{3.2}$$

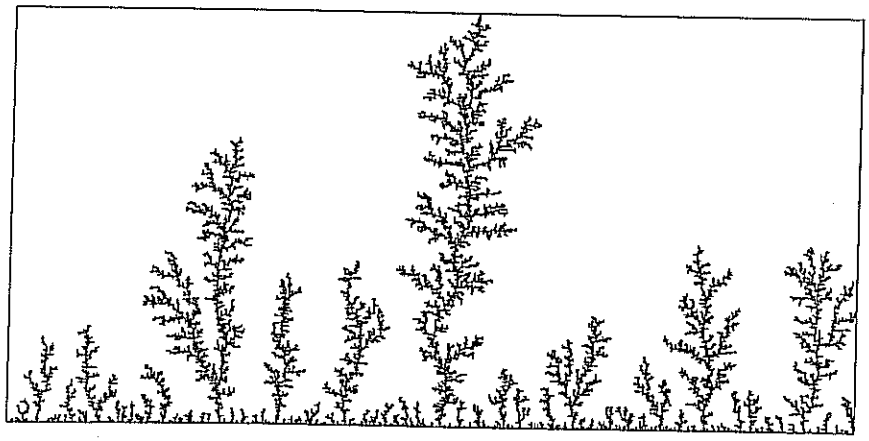

Figure 6. A DLA grown on linear base (courtesy A. Arnéodo). At this stage of the growth only the largest structures are still growing, the others are screened off.

In the standard model there is no surface tension and the growth is unstable at all scales. However, the numerical technique itself, because it always uses a lattice or particles of finite size, introduces a length scale l_u: the lattice mesh or the particle size. The role of this discretization is evident at the first stages of the growth shown on figure 6: the first layer deposited on the baseline is lacunary at a scale of the order of l_u. Several works (Viczek 1984; Sarkar 1985; Sander, Ramanlal & Ben Jacob 1985; Kadanoff 1985; Liang 1986) have been devoted to variants of DLA in which the rules are changed so as to introduce an effective surface tension. The small length scale then becomes larger than l_u and the patterns are more similar to Saffman–Taylor fingering.

3.2 Solidification instability

The solidification problem is treated in Chapter 8. We present here only its main results in order to underline the similarities and differences of this instability with viscous fingering. Crystals can be grown either from a melt or from a solution (Langer 1980 and Caroli, Caroli & Roulet 1992). Experimentally the growth of a crystal in either of these situations occurs when the system loses equilibrium through undercooling. We limit ourselves here to considering the growth in a melt.

The solidification of a pure melt occurs when the temperature T_∞ imposed on the fluid is below the temperature T_f of equilibrium between the liquid and the solid. The undercooling is $\Delta = T_f - T_\infty$. As the solid grows into

the liquid, it releases latent heat: a diffusive temperature field is formed in front of the crystallization front. It is controlled by two Fourier equations of diffusion, one on each side of the interface:

$$\frac{\partial T}{\partial t} = D_T^i \nabla^2 T. \tag{3.3}$$

The scalar field here is the temperature and D_T^i is the heat diffusion coefficient, for the liquid ($i = 1$) or the solid ($i = 2$) respectively.

The heat produced by the solidification is diffused on both sides of the interface; this provides a relation between the growth velocity and the temperature gradients:

$$LV_n = \left[D_T^1 C_p^1 (\nabla T)_1 - D_T^2 C_p^2 (\nabla T)_2\right] \cdot \boldsymbol{n}, \tag{3.4}$$

where L is the latent heat, V_n the normal velocity of the front, and C_p^1 and C_p^2 the heat capacity of the solid and the liquid respectively. The two diffusion constants are usually taken to be equal (symmetrical model).

Finally, the melting temperature of the solid is modified when the interface is curved by the pressure induced by capillarity. This is the Gibbs–Thomson effect. The equilibrium temperature is changed:

$$T = T_f \left(1 - \frac{\gamma\kappa}{L}\right), \tag{3.5}$$

where γ is the surface tension and κ the curvature of the interface ($\kappa > 0$ if the centre of curvature is in the solid). It is found that only at undercooling $\Delta = L/C_p^1$ is the plane front a solution for a forced growth at constant V_n.

The solidification process is *a priori* associated with two length scales: the diffusion length scale $l_D^T = D_T/V$ and the capillary length scale d_0. This latter scale is the size of the smallest crystal in equilibrium in the melt at the given temperature: it is related to L, the latent heat of solidification, γ, the surface tension, and C_p, the heat capacity through

$$d_0 = \frac{\gamma C_p T_f}{L^2}. \tag{3.6}$$

The linear analysis of the stability of the plane solidification front in a pure melt is due to Mullins & Sekerka (1964). It shows that it is unstable at all velocities but that small scales are stabilized by capillary effects through the Gibbs–Thomson effect. As demonstrated in Chapter 8, in the situation where equation (3.3) can be approximated by Laplace's equation, the amplification rate of a perturbation of wave-vector k is

$$\sigma = V|k|\left(1 - \frac{D_T}{V} d_0 k^2\right), \tag{3.7}$$

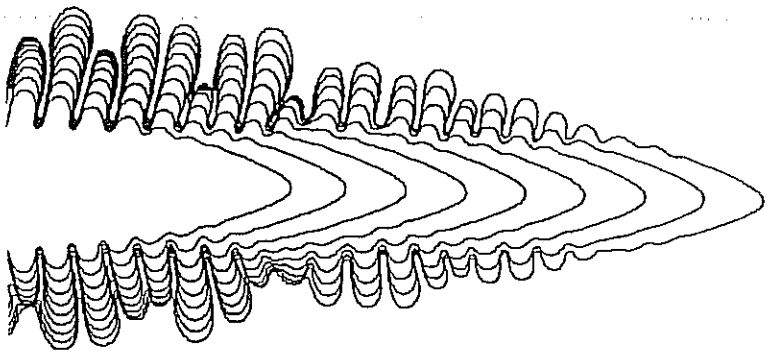

Figure 7. The growth of a parabolic dendritic monocrystal (from Dougherty & Gollub 1988).

a relation comparable to that found by Chuoke *et al.* (1959) for viscous fingering (see equation (2.26) and figure 5). The maximum instability of a front growing at velocity V occurs at

$$l_c^s = 2\pi\sqrt{\frac{3D_T d_0}{V}} = 2\pi\sqrt{3l_D^T d_0}, \tag{3.8}$$

which is the length scale of the instability; it is proportional to the geometrical mean of the two physical scales l_D^T and d_0.

In most real solidification processes the impurities rejected by the solid form a diffusive field in front of the crystal. As the molecular diffusion constant D_c is much smaller than D_T most crystallization processes are controlled by the impurity diffusion field. An important difference with the above case is that while the diffusion of heat is almost equal in the solid and the liquid, the diffusion of impurities is large in the solution and small in the solid. A linear stability analysis was performed by Langer (1980) in this case. Its results are similar to those obtained by Mullins & Sekerka. The maximum instability occurs at a length scale l_c^{sc} proportional to the geometrical mean between the impurity diffusion length $l_D^c = D_C/V$ and a chemical capillary length d_0'. Like viscous fingering, this linear analysis only gives a length scale for the problem. Experimentally, the plane growth only exists transitorily but the length scale l_c^{sc} retains its importance in the case of the needle crystals called dendrites. One of them is shown on figure 7. They will be described in § 4.2.

3.3 Other systems

As already stated, many phenomena belong to this class of processes. We shall here quote two more. The growth of bacterial colonies (Fujikawa &

Matsushita 1991; Ben Jacob *et al.* 1992) takes place in a Petri dish filled with an agar–agar gel containing a weak concentration of nutrient. In the middle of the cell a small number of bacteria are deposited. As the bacteria start proliferating they deplete the concentration of nutrient in their vicinity. This depletion of the concentration tends to be compensated by molecular diffusion. The bacteria which are at the periphery of a protrusion will be located in a stronger gradient, will receive more food and will thus proliferate. Once again the scheme of figure 2 is relevant: the interface is unstable and the tips grow faster.

Other systems generate other types of morphologies as they belong to a different class. For instance the breaking of a window pane generates a pattern of propagating cracks. The dynamics of fractures, widely investigated recently (see Hull 1999 for a review), occurs in a stress field which is modified by its progression. It is thus also a free boundary problem. However, the morphologies observed are very different. For instance the breaking of a glass plate is characterized by the formation of both radial and orthoradial cracks meeting at right angles. The origin of the difference in the morphologies lies in the fact that the stress field in which the cracks propagate is tensorial instead of scalar.

4 The existence of stable curved fronts

The instability of the plane fronts in all these systems does not preclude the possibility of existence of stable steady solutions of different shapes. Such fronts are observed experimentally and the search for stable curved fronts actually preceded the linear stability analysis of the plane ones. Two cases have been the focus of interest: the Saffman–Taylor finger and the parabolic needle crystal.

4.1 Isotropic case

Most of the knowledge we have on non-fractal isotropic growth comes from viscous fingering and was obtained in two geometries. In the first, introduced by Saffman & Taylor (1958), the two fluids move in a Hele-Shaw cell in the shape of a long linear channel closed on both lateral sides. In the second, used by Thomé *et al.* (1989), the fluids move between two walls forming a wedge.

4.1.1 Linear channel

This configuration has translational invariance along the cell. The nature of the pattern observed is controlled by a parameter B proportional to the

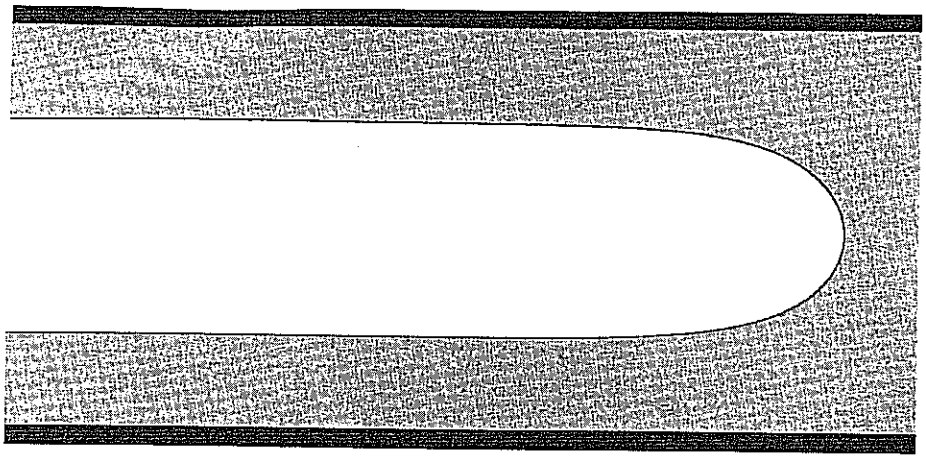

Figure 8. Photograph of Saffman–Taylor finger of width $\lambda = 0.5$ obtained in a linear channel at $B \approx 2 \times 10^{-4}$.

square of the ratio of the small scale (l_c, the length scale of the instability (2.28)) to the large scale (the width W of the channel). It is traditionally chosen as:

$$B = \frac{\gamma}{12\mu V}\left(\frac{b}{W}\right)^2 = 8.45 \times 10^{-3}\left(\frac{l_c}{W}\right)^2. \tag{4.1}$$

For a large range of values of B one single finger is observed to move steadily along the cell with a well-defined width and shape as shown on figure 8. As B decreases, the ratio λ of the finger width to the channel width tends towards $\lambda = 0.5$. This situation persists (Tabeling *et al.* 1987) down to values of $B \approx 1.4 \times 10^{-4}$ i.e. for $W \approx 8l_c$. For $B < 1.4 \times 10^{-4}$ the finger becomes unstable as described in § 5.1.2.

Saffman & Taylor (1958) showed that it was possible, if surface tension was neglected, to find by conformal transform techniques a family of analytical solutions for finger-shaped interfaces. Their theory can be summarized as follows. The finger and the channel are drawn in figure 9(*a*). The origin of the axes is at the finger tip, the walls are respectively at $y = \pm 1$ and the finger has two asymptotes at $y = \pm\lambda$ (the channel and the finger width are here 2 and 2λ respectively). The velocity of the finger is U and the velocity of the fluid far from the finger is V. If the finger width is λ, then $V = \lambda U$. The velocities given by equation (2.5) derive from potentials

$$\phi_i = -\frac{b^2}{12\mu_i} p_i. \tag{4.2}$$

It is possible to define stream functions ψ_i such that

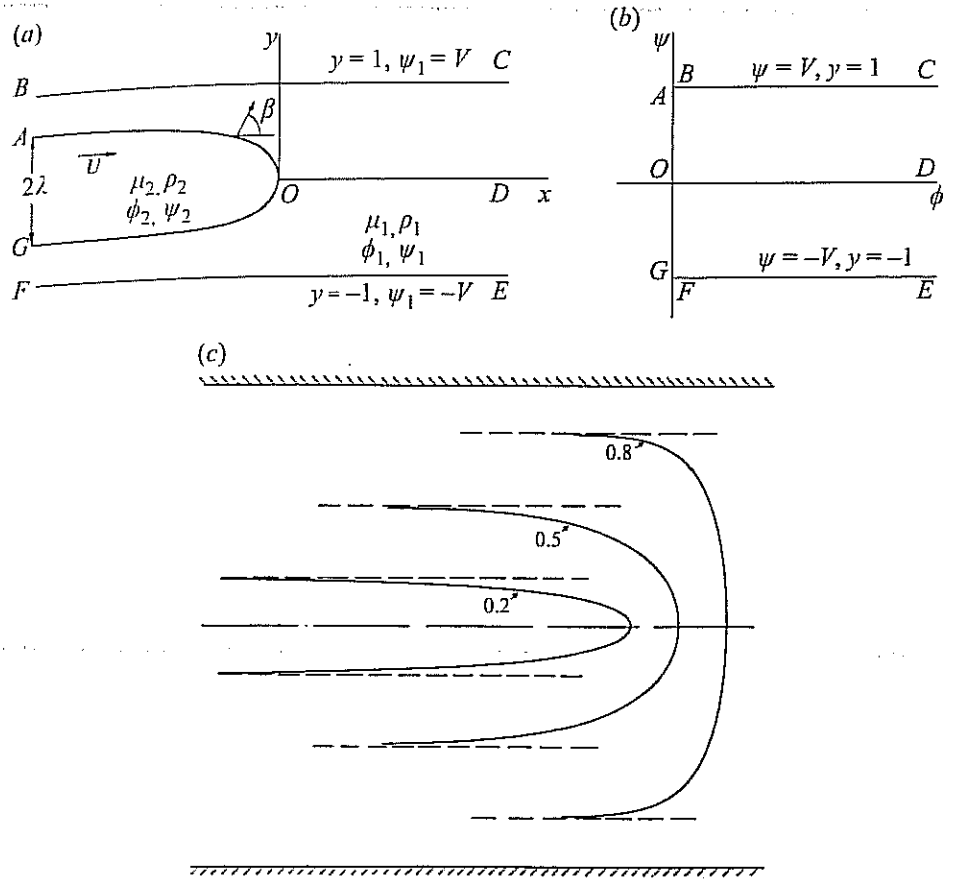

Figure 9. (*a*, *b*) Diagrams (from Saffman & Taylor 1958) showing the boundaries respectively in physical space and in the (ϕ, ψ)-plane. (*c*) Three finger profiles of the continuous family of solutions given by equation (4.8) (from Saffman & Taylor 1958).

$$u_i = \frac{\partial \phi_i}{\partial x} = \frac{\partial \psi_i}{\partial y}, \qquad v_i = \frac{\partial \phi_i}{\partial y} = -\frac{\partial \psi_i}{\partial x}. \tag{4.3}$$

Since the flow corresponds to a Laplacian field, the complex potential $\omega = \phi + i\psi$ is an analytic function of $z = x + iy$. The continuity of the normal components of the velocity at the interface can be written:

$$\frac{\partial \phi_1}{\partial n} = \frac{\partial \phi_2}{\partial n} = U \cos\beta, \tag{4.4}$$

where β is the angle between the x-axis and the normal $\boldsymbol{n}$ to the interface. On the surface of the finger, $\partial\phi/\partial n = \partial\psi/\partial s$ where s is the curvilinear position

along the interface. Since $\cos\beta = \partial y/\partial s$, we have on the surface of the finger,

$$\psi_1 = \psi_2 = Uy. \tag{4.5}$$

In the absence of surface tension the continuity of pressure through the interface gives

$$\phi_1 = \phi_2 = 0. \tag{4.6}$$

On the walls ($y = \pm 1$), $\psi = \pm V$ and at infinity in front of the finger $\phi = Vx$. The problem is then transferred into the (ϕ, ψ)-plane (figure 9*b*) and the trick is to consider $x + \mathrm{i}y$ to be an analytic function of $\phi + \mathrm{i}\psi$. On this plane the surface of the finger is mapped onto the segment AG so that there is no longer a free boundary, and the walls of the channel map onto $\psi = \pm V$ with $\phi > 0$. The function satisfying the boundary conditions is

$$z = \frac{\omega}{V} + \frac{2}{\pi}(1-\lambda)\ln\frac{1}{2}\left[1 + \exp\left(-\frac{\pi\omega}{V}\right)\right], \tag{4.7}$$

which determines the potential as a function of z. The shape of the interface is found by setting $\phi = 0$ in equation (4.7). Written in dimensional variables, W being the width of the channel,

$$x = \frac{W(1-\lambda)}{2\pi}\ln\frac{1}{2}\left[1 + \cos\left(\frac{2\pi y}{\lambda W}\right)\right]. \tag{4.8}$$

These fingers are parameterized by their relative width λ which can take any value from 0 to 1 (figure 9*c*). The shape of the solution of width 0.5 fits the experimentally observed finger (figure 8) extremely well.

The remaining problem was that no reason was found at the time for the selection of this particular solution. The answer to this question came much later and was obtained by investigating the role of surface tension. This analysis is too long to be reproduced here; we will only summarize its results. The selection was first obtained in numerical investigations by McLean & Saffman (1981), Schwartz & Degregoria (1987) and Vanden-Broeck (1983) and fully understood in analytic works by Combescot *et al.* (1986, 1988), Hong & Langer (1986), and Shraiman (1986). Surface tension cannot be treated as a perturbation because it introduces higher-order terms in the integro-differential equation defining the interface. When the transcendentally small terms due to surface tension are taken into account, the requirement that the finger should be smooth at the tip introduces a solvability condition. For a given value of B there is only one discrete set of solutions of width λ_n for which this condition is satisfied; they all tend to have a width 0.5 for vanishing B. In the limit of very low B, their dependence

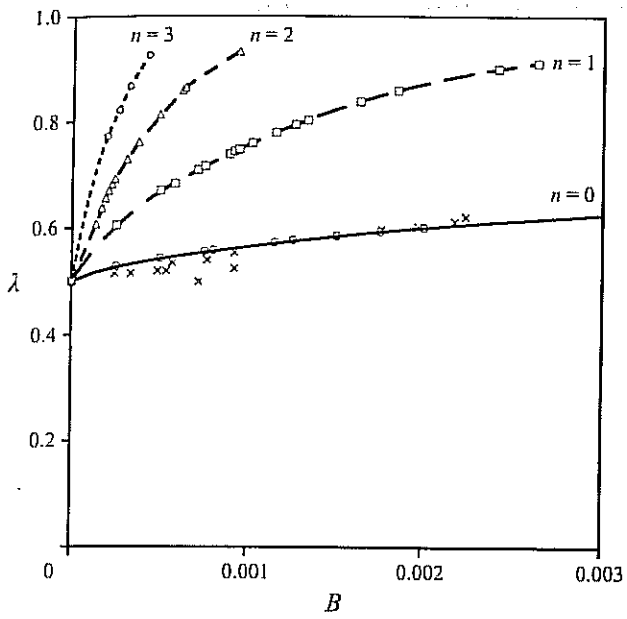

Figure 10. The B-dependence of the widths of the discrete set of solutions selected by surface tension. The open symbols result from numerical simulation (courtesy M. Ben Amar), the crosses are the finger widths measured by Saffman & Taylor (1958).

on B is given analytically by

$$\left(\lambda_n - \tfrac{1}{2}\right) = \left(\tfrac{1}{8}\right) a_n \left(16\pi^2 B\right)^{2/3}, \tag{4.9}$$

where the coefficients a_n are related to the successive integers n by

$$a_n = 2(n + 4/7)^2. \tag{4.10}$$

This dependence can also be found numerically. Figure 10 shows the evolution of these solutions as a function of B. The stability of the various branches was investigated by Bensimon, Pelcé & Shraiman (1987), Tanveer (1987*b*) and Kessler *et al.* (1988): only the lower branch is stable, the others are unstable through tip splitting.

The singular characteristic of this selection is demonstrated by the fact it can be removed experimentally by various types of very localized and small disturbances of the finger tip (Couder *et al.* 1986*b* and Rabaud, Couder & Gerard 1988). When this is done the normal Saffman–Taylor finger is replaced by a narrower and faster finger. This is a direct experimental confirmation of the singular role ascribed by the theory to the finger tip. The new structure, often called an anomalous finger, will be discussed in § 4.2.2.

Finally we can note that it is possible to introduce for DLA growth an equivalent to surface tension (by using specific rules for the sticking of particles on the aggregate). Kadanoff (1985) and Liang (1986) have shown that it was thus possible to recover the stable isotropic Saffman–Taylor finger in a linear channel.

4.1.2 Sector-shaped cells

In a sector-shaped cell the viscous finger moves between two lateral walls forming an angle θ_0. By convention the angle of the wedge θ_0 is considered positive when the finger moves in the divergent direction, the situation mainly considered here. The parameter controlling the growth is chosen, by analogy with the linear channel, as $B = 8.45 \times 10^{-3}(l_c/\theta_0 r)^2$ where $r\theta_0$ is the curvilinear local width $W(r)$. For moderate values of B a single finger is observed which occupies a finite fraction $\lambda_{\theta_0} > 0.5$ of the angular width of the wedge (figure 11*a*). This fraction λ_{θ_0} is approximately a linear function of the wedge angle (figure 11*b*). The finger grows as a self-similar structure if and only if B is kept constant, i.e. if the velocity V decreases as r^{-2}. In most practical cases V is constant, so the finger is observed to become spontaneously unstable (figure 11*a*).

The theoretical treatment of this situation followed the same path as that of the linear case. Neglecting surface tension, a set of self-similar solutions was first found for $\theta = 90°$ (V. Hakim in Thomé *et al.* 1989). Then for any value of θ_0, families of solutions given by hypergeometric functions and again parameterized by their width λ_{θ_0} were found by Ben Amar (1991*a*). The selection due to isotropic surface tension was investigated both numerically (Ben Amar *et al.* 1991, Ben Amar 1991) and analytically by Combescot & Ben Amar (1991). For a given value of B there is again selection of a discrete set of solutions. The evolution of this set as a function of B is given for the wedge with $\theta_0 = 20°$ in figure 12 where it can be compared with that of the parallel channel. The comparison shows that the selected widths λ_{θ_0} are shifted to larger values. Furthermore the levels $n = 0$ and $n = 1$ coalesce at a value B_l so that they form a loop and do not exist for $B < B_l$. The experimental observations show that when moving at constant velocity the finger adapts constantly to the evolution of the local parameter B as defined in the tip region. The finger is first stable, with a slowly varying width given by that of the level $n = 0$. When the local B reaches the limit value B_1, the finger becomes unstable.

Taken together, the results obtained in the linear and sector-shaped cells show that: (i) for an isotropic interface the selection process defines the finger width, and the selection occurs at the large scale of the system; (ii)

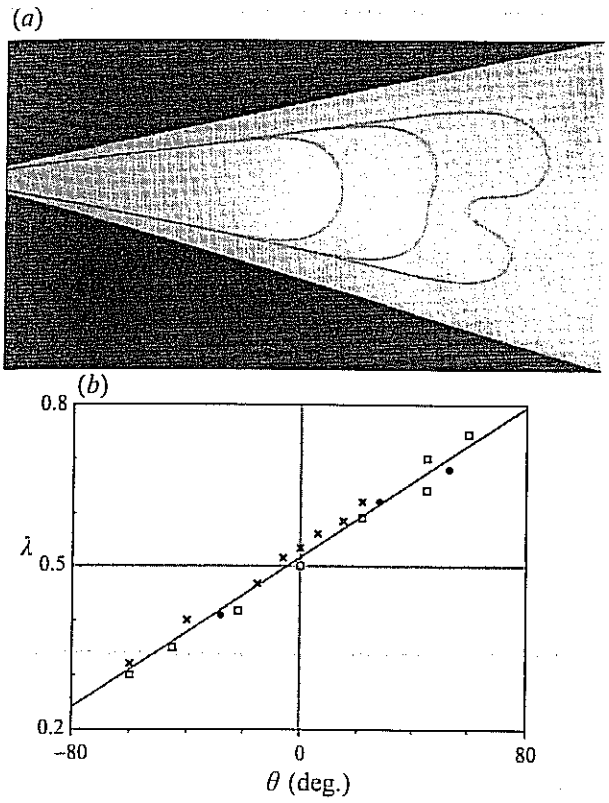

Figure 11. (*a*) Three superposed photographs of the evolution of a Saffman–Taylor finger of width $\lambda = 0.66$ obtained in a sector-shape-cell of angle $\theta_0 = 30°$. (*b*) The crosses are the width of the stable fingers as a function of the angle θ_0 at $B \sim 10^{-3}$. The open squares are the width of ensemble-averaged unstable Saffman–Taylor fingers. The black diamonds are the width of ensemble-averaged DLA grown in wedges.

the global curvature imposed by the geometry affects the selection and the stability of the finger.

4.1.3 Circular geometry

In the axisymmetric geometry (see figure 1), at the very beginning of the air injection, the interface is circular. When the perimeter of this circle becomes large enough the front destabilizes spontaneously at the scale l_c and a small number (usually 5 to 7) of radially growing fingers are formed. Each of these fingers resembles the fingers obtained in wedges. This analogy can be made quantitative (Thomé *et al.* 1989). Each finger grows as if it were enclosed in a cell, having virtual walls formed by the bisectors of the region separating

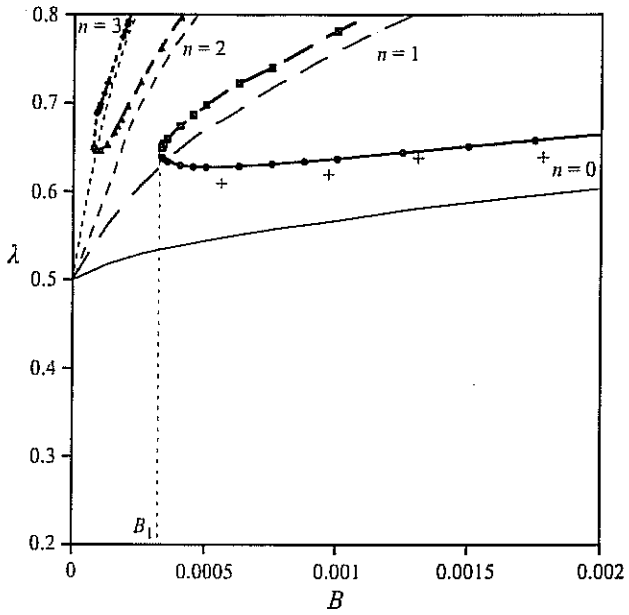

Figure 12. The B-dependence of the widths of the discrete set of solutions in a wedge of angle $\theta_0 = 20°$ (thick lines). The thin lines show for comparison the discrete set in the linear cell. The crosses are experimental results.

this finger from its two neighbours. With this rule the shape, the width and the stability of each finger can be predicted by the results obtained for sector-shaped cells. Since in practical situations the growth occurs at constant velocity, the local B decreases and there will be a constant unsteady evolution of the pattern. As they continue to grow the fingers destabilize and tend to form increasingly complex 'trees'. However, even when the growth has formed a fractal object, the initial breaking of the symmetry still appears to persist and to be at the origin of the formation of independent trees.

4.2 Non-isotropic situation

Non-isotropic growth can be obtained in the three types of experiments described here. We will first briefly describe its archetype which is the dendritic growth of crystals (for reviews see Huang & Glicksman 1981 and Pomeau & Ben Amar 1992). Then we will show that anomalous Saffman–Taylor fingering in the presence of localized disturbances is a similar type of growth.

4.2.1 The dendrite

The structures formed during the crystallization of a solution or a melt are dendrites of the type shown on figure 7 (provided this crystallization is not too slow). Each dendrite is a monocrystal growing in a well-defined direction and having a parabolic tip. This growth direction is one of the main axes of the crystal lattice. At some distance from the tip the curved front becomes unstable and there is formation of lateral branches which grow along other main crystallographic directions of the crystal. The theoretical analysis of dendritic growth has a history somewhat similar to that of Saffman–Taylor fingering. We limit ourselves here to a brief recalling of results in the case closest to the Laplacian problem, namely a two-dimensional situation where there is only diffusion on one side of the interface, a condition well satisfied in the case of impurity diffusion. This also limits considerations to cases where the diffusion length is very large compared to the crystal size and where the boundaries are far away. It was shown by Ivantsov (1947) that, in the absence of surface tension, parabolas were possible stationary solutions of the shape of the interface separating the solid and the liquid. As in the Saffman–Taylor problem the argument gave no hint as to the selection of the experimentally observed solution. In the case of dendrites there is still no selection mechanism known when isotropic surface tension is taken into account (Kessler, Koplik & Levine 1986*a* and Caroli, Caroli & Roulet 1987). However, crystals are anisotropic and the surface tension γ of the interface is a function of the angle Θ of the normal to the interface with the main axis of the crystal. For a cubic crystal

$$\gamma = \gamma_0(1 + \epsilon\cos\Theta). \tag{4.11}$$

If this anisotropy of the surface tension is taken into account, a discrete set of parabolas is selected for a given undercooling (Ben Amar 1990). The observed solution is the fastest one. It is defined by its radius of curvature r_d which is proportional to the instability length scale l_c^{sc} (§ 3.2). The coefficient of proportionality is a function of the anisotropy ϵ. In the limit of very weak anisotropy the theoretical result can be written

$$r_d = 0.5\epsilon^{-7/8} l_c^{sc}. \tag{4.12}$$

This type of selection has been confirmed by Dougherty & Gollub (1988) and Maurer, Perrin & Tabeling (1991) but the experimental measurement of ϵ is very difficult so that the dependence on ϵ has not yet been confirmed experimentally.

It is worth mentioning that Honjo, Ohta & Matsushita (1986) have shown that the presence of very strong external noise could destroy the effect of

anisotropy. No dendritic growth of the crystal is then observed and the growth appears isotropic.

4.2.2 The anomalous Saffman–Taylor finger

A comparison of the two types of growth, viscous fingers or dendrites, described above leads one to ask whether their difference is linked with the difference in their physical nature or simply to a difference in their symmetries. Is it possible to obtain viscous fingers which look like dendrites? A positive answer to this question is given when preferential directions of growth are imposed on viscous fingering. A global disturbance can be imposed by using glass plates deeply engraved with a periodic lattice of grooves (Ben Jacob *et al.* 1985; Chen & Wilkinson 1985) or replacing the viscous fluid by an anisotropic liquid crystal (Buka, Kertesz & Vicsek 1986). In fact, since the selection is a singular effect occurring at the tip, a single disturbance localized in this region is sufficient to upset the growth (Couder *et al.* 1986*a*, *b*). In the radial configuration all these disturbances result in fingers which grow faster than normal, have stable tips and exhibit dendritic-like side branches. In linear channels the difference is more striking and easier to study quantitatively. Figure 13(*a*) shows a finger obtained in a linear channel in which the local disturbance is created by a thin groove engraved along the axis of each of the two glass plates (Couder *et al.* 1986). The observed fingers are much narrower than usual (for instance $\lambda = 0.22$ on figure 13*a*). Their shapes are however still very well fitted by the Saffman–Taylor analytical solutions of the same width λ (4.8) so that a quantitative study is possible.

The selection of these anomalous fingers (Rabaud *et al.* 1988) is clearly different from that in the isotropic case. Fingers grown at the same velocity in channels of different width have very different λ but a similar tip. As the finger shapes are given by equation (4.8) the radius of curvature at the tip r_{ST} can be deduced from the measured λ:

$$r_{ST} = \frac{\lambda^2 W}{\pi(1-\lambda)}. \tag{4.13}$$

Anomalous fingers grown in various cells at the same velocity with the same disturbance have the same r_{ST}. On varying the velocity, r_{ST} is found to be proportional to the capillary length scale (figure 13*b*):

$$r_{ST} = \alpha l_c. \tag{4.14}$$

The value of the coefficient α is observed to be dependent on the strength of the applied disturbance. Relation (4.14) is similar to (4.12), meaning that

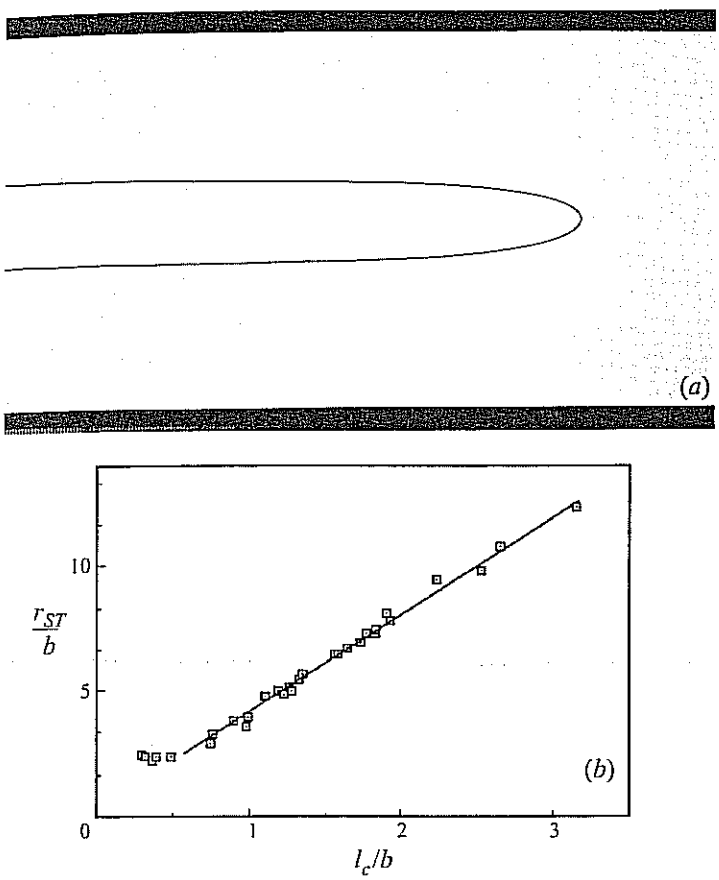

Figure 13. (*a*) A photograph of an anomalous finger of width $\lambda = 0.22$ obtained in a linear channel when one of the glass plates has a single groove etched along its axis. (*b*) A graph of the radius of curvature of the tip r_{ST}/b versus l_c/b (Rabaud *et al.* 1988). The saturation occurs when $r_{ST} \approx 2.5b$ where the two-dimensionality breaks down.

anomalous fingers are not only visually similar to dendrites, they also obey the same selection rules. This situation has now been widely investigated experimentally (Kopf-Sill & Homsy 1987; Zocchi *et al.* 1987; Rabaud *et al.* 1988), numerically (Dorsey & Martin 1987; Sarkar & Jasnow 1989) as well as theoretically (Hong & Langer 1986, 1987; Combescot & Dombre 1989).

The numerical simulations show that in the presence of anisotropy parallel to the channel, the lower level of the discrete set does not tend towards $\lambda = 0.5$ but towards $\lambda = 0$ as shown on figure 14. This regime is observed in a limited domain of values of the parameter B. There are two crossovers, respectively at very low and very high velocities. A very slowly growing

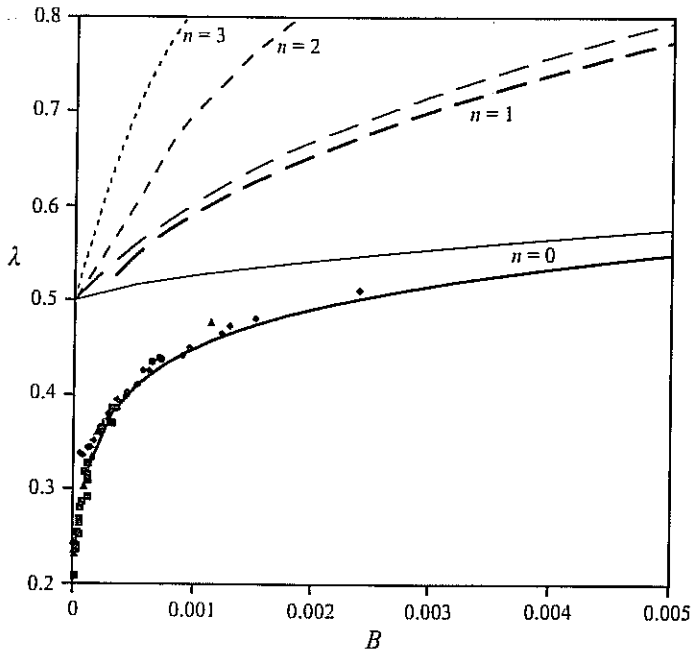

Figure 14. The B-dependence of the width of the discrete set of solutions in the presence of anisotropy (thick lines). Black symbols: measured width of fingers obtained with a given disturbance of the tip. The thin lines show the discrete set in the linear cell.

finger is only weakly affected by anisotropy and its width remains close to that of the isotropic one. (This crossover is similar to that investigated for crystals grown in a narrow channel (Kessler *et al.* 1986*b*).) For very fast growing fingers when the tip radius of curvature becomes of the order of the thickness of the cell (at $r_{ST} \approx 2.5b$) saturation is observed (figure 13*b*). This corresponds to the breakdown of the two-dimensional behaviour.

The selection process of normal Saffman–Taylor fingers has been removed mainly by disturbances that affect the isotropy or the homogeneity of the interface; this is the most common situation and the most relevant to an analogy with crystal growth. However, since this selection is due to a delicate relation between an isotropic surface tension and a hydrodynamic flow, it can also be removed by a disturbance of the flow only, the interface remaining isotropic. This was suggested theoretically by Combescot & Dombre (1989) and experimentally confirmed by Thomé, Combescot & Couder (1990) in experiments in which the flow, ahead of the finger, is disturbed by a moving disk.

Taken together the results for both the anomalous Saffman–Taylor fingers and the dendritic growth show that either a local disturbance or anisotropy results in a selective process which defines the radius of curvature at the finger tip. The selection thus occurs at the small scale of the system.

4.3 The stability of the curved fronts

Both the Saffman–Taylor and the solidification instabilities generate structures, fingers or dendrites, which are curved fronts that can have steady solutions but can also become unstable. It is thus necessary to examine specifically the problem of the stability of curved fronts. This was first undertaken by Zel'dovich *et al.* (1980) in the context of flame fronts. A review of this problem can be found in Pelcé (1988). The results presented above have shown that the selection mechanisms at work in the isotropic or anisotropic cases lead respectively to the tip being of small or strong curvature respectively compared to the typical length scale. For this reason the type of instability observed in the two cases is very different.

4.3.1 Isotropic case

Isotropic curved fronts are selected to be on the scale of the channel width. Naively, decreasing B means that the finger tip becomes wider and wider in relation to l_c. The finger front will thus be increasingly similar to a straight front and tend to be unstable at the capillary length l_c corresponding to the local normal component of the velocity. This is observed in wedges where the experiments (Thomé *et al.* 1989) show that the finger is destabilized more and more easily through tip splitting for increasing angles. For each angle, the finger is destabilized (figure 11*a*) when the local value of B at the finger tip reaches the value B_1 for which the lower level $n = 0$ ceases to exist (figure 12). By contrast, in the linear channel the finger is stabilized by its curvature and Bensimon *et al.* (1987) and Tanveer (1987*a*) found the lower branch $n = 0$ of figure 10 to be linearly stable while the other branches were unstable. Experimentally, however, for B values smaller than 1.4×10^{-4}, the observed finger is unstable to tip splitting (figure 15*a*). This can be ascribed to the fact that as B tends to zero the branches become more closely spaced and the natural noise is enough to induce a subcritical transition to one of the neighbouring unstable states.

4.3.2 Anisotropic case

For non-isotropic fronts, dendrites or anomalous fingers, the finger tip is defined by the small scale. On decreasing B, the tip radius of curvature r_{ST}

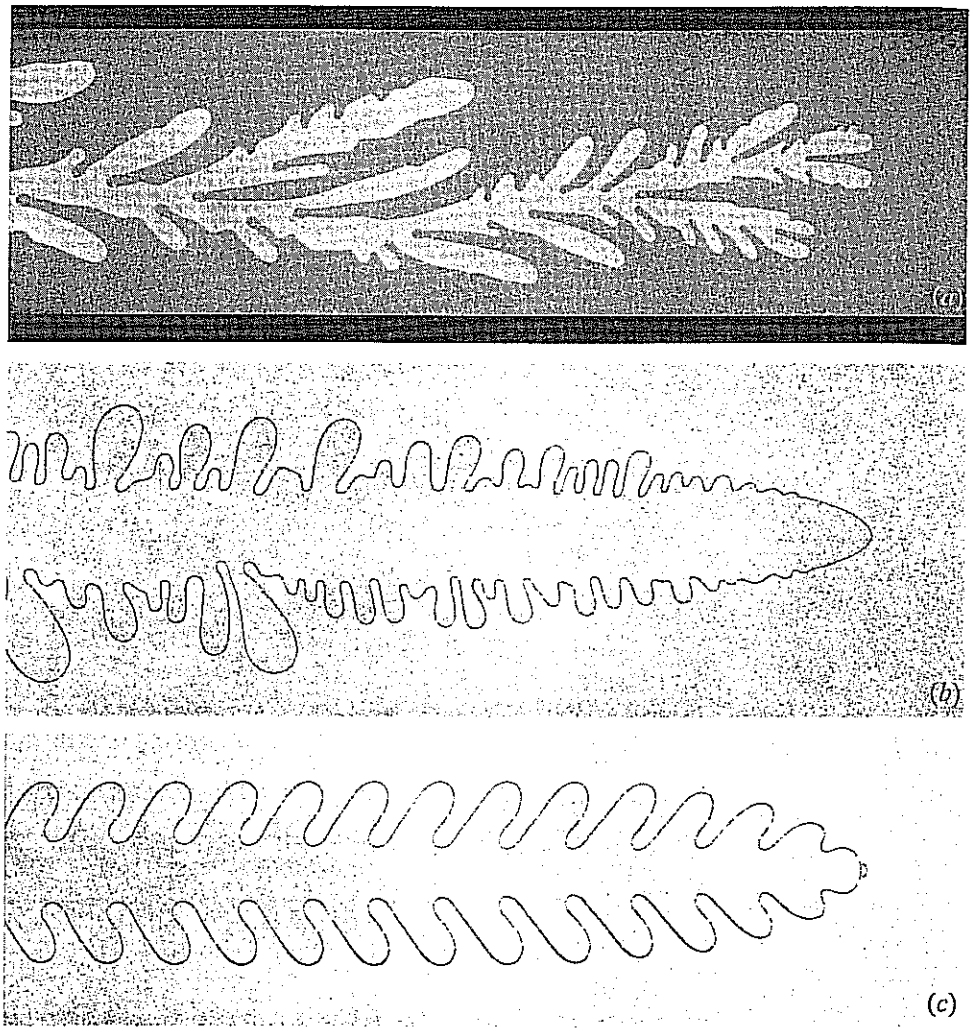

Figure 15. (*a*) A very unstable isotropic finger in a linear cell. (*b*) The natural instability of an anomalous Saffman–Taylor finger grown in a wide channel (Rabaud *et al.* 1988) to be compared with the dendrite on figure 7. (*c*) An anomalous Saffman–Taylor finger subjected to a periodic forcing.

always remains in the same ratio to the capillary length scale; when the anisotropy is large the tip is thus observed to be stable. The same is not true of the lateral sides. They are always unstable to dendrites (figure 7). For anomalous viscous fingers, as the scale of r_{ST} moves away from the scale of W, the relative width of the finger λ decreases and the finger profile becomes parabolic in a larger and larger region behind the tip. As a result a lateral

instability grows (figure 15*b*). It is identical in nature to the lateral instability of crystalline dendrites (figure 7).

The specificity of the growth of an instability advected along a curved front was first pointed out by Zel'dovich *et al.* (1980) in the context of flame fronts. The growing wave, being advected along a curved front, is stretched by a kinematic effect due to the growing tangential velocity. This effect was investigated by Pelcé & Clavin (1987) and Kessler & Levine (1987). A second effect was pointed out by Caroli *et al.* (1987): each region of the front is unstable through a process described by the linear stability analysis of equation (2.26) or (3.7). Along the curved fronts the normal velocity decreases continuously away from the tip. As a result there is a continuous shift of the maximum amplification rate towards larger wavelengths. Both effects tend to increase the wavelength away from the tip.

The most important point that underlies these arguments is that the side branching is an instability of a convective type. This means that it has a spatial growth rather than a temporal one (for a discussion of absolute and convective instabilities see Chapter 4). This was first demonstrated in anomalous Saffman–Taylor fingers because they can be manipulated easily. Rabaud *et al.* (1988) gave a sudden local disturbance to the tip of an anomalous finger and showed that it resulted in the growth of a wave packet which, in the frame of reference of the finger, was advected away from the unstable region. No waves remained in the front region so that any later disturbance was uncorrelated with an earlier one. This is precisely the characteristic of a convective instability. Furthermore this experiment permitted the direct observation of the wavelength change along the profile due to both the Zel'dovich stretching and the shift in wavelength selection. The same demonstration was done in the case of dendritic growth by Quian & Cummins (1990) using a laser pulse to disturb the tip.

The main characteristic of convectively unstable media is that they behave as a selective amplifier of the noise. This is precisely the characteristic that Dougherty & Gollub (1988) demonstrated experimentally for the dendritic side branching. But in convective instabilities noise can be replaced by a periodic forcing of larger amplitude. The instability is thus made strictly periodic at the imposed frequency. A strictly periodic side branching is observed when the input pressure is modulated and acts as a forcing frequency. It is worth noting that similar periodic side branches are obtained spontaneously with a small bubble at the finger tip because it forms a small local oscillator (figure 15*c*). A similar temporal forcing was applied to a growing dendrite by Bouissou *et al.* (1990) by imposing a modulated flow around the dendrite tip.

5 Fractal structures

We can now return briefly to open geometries in which the large scale is not fixed but is of the order of the size of the pattern itself, becoming constantly larger as it grows. Figures 16(*a*) and 16(*b*) show two large patterns grown in a DLA simulation and in a Saffman–Taylor fingering experiment respectively. Both exhibit a very complex structure with a hierarchy of branches of different sizes. A classical question about complex structures is whether or not they have a fractal structure.

The fractal objects first investigated were mathematically defined self-similar structures built with an iterative scaling construction rule (for reviews see for instance Mandebrodt 1982 and Vicsek 1989). One of the characteristics of such mathematical fractals embedded in a space of dimension d is their fractal dimension d_f. This dimension is usually obtained by the box-counting method. The number $N(\epsilon)$ of d-dimensional boxes necessary to cover the whole pattern is measured as a function of the size ϵ of these boxes. We then plot $\log(N(\epsilon))$ as a function of $\log(\epsilon)$. For a mathematical fractal this plot gives a linear dependence showing that the ϵ-dependence of N is of the form

$$N(\epsilon) \propto \epsilon^{-d_f}, \tag{5.1}$$

where d_f is the structure's fractal dimension.

It has become habitual now, whenever a complex physical structure is observed, to do some image processing and to seek a scaling of the type of equation (5.1). In the case shown on figure 16(*a*, *b*) the plots of $\log(N(\epsilon))$ as a function of $\log(\epsilon)$ exhibit a well-defined linear behaviour in a range roughly falling between L and l_c (or l_u). In this range the slope of the plot is approximately $d_f = 1.67$ so that these patterns are said to be fractals. Muthukumar (1983) and Tokuyama & Kawasaki (1984), using different theoretical arguments, proposed that DLA grown in a plane should have $d_f = 5/3$, a value close to what is found numerically. It should be underlined that in all physical fractals the domain of fractal behaviour is bounded. In the present case, for length scales larger than L the slope of the log − log plot tends to zero because on very large scales the pattern is similar to a point. For very small scales there is another crossover to a slope −2: the pattern on these scales is a two-dimensional object. The fractal behaviour in growth patterns is thus best observed when the two typical length scales are furthest from each other. For this reason DLA serves as a good model for fractal growth because it provides the largest fractal range. It is mostly investigated in the radial configuration and can be either isotropic as shown in figure 16 or anisotropic as in figure 18.

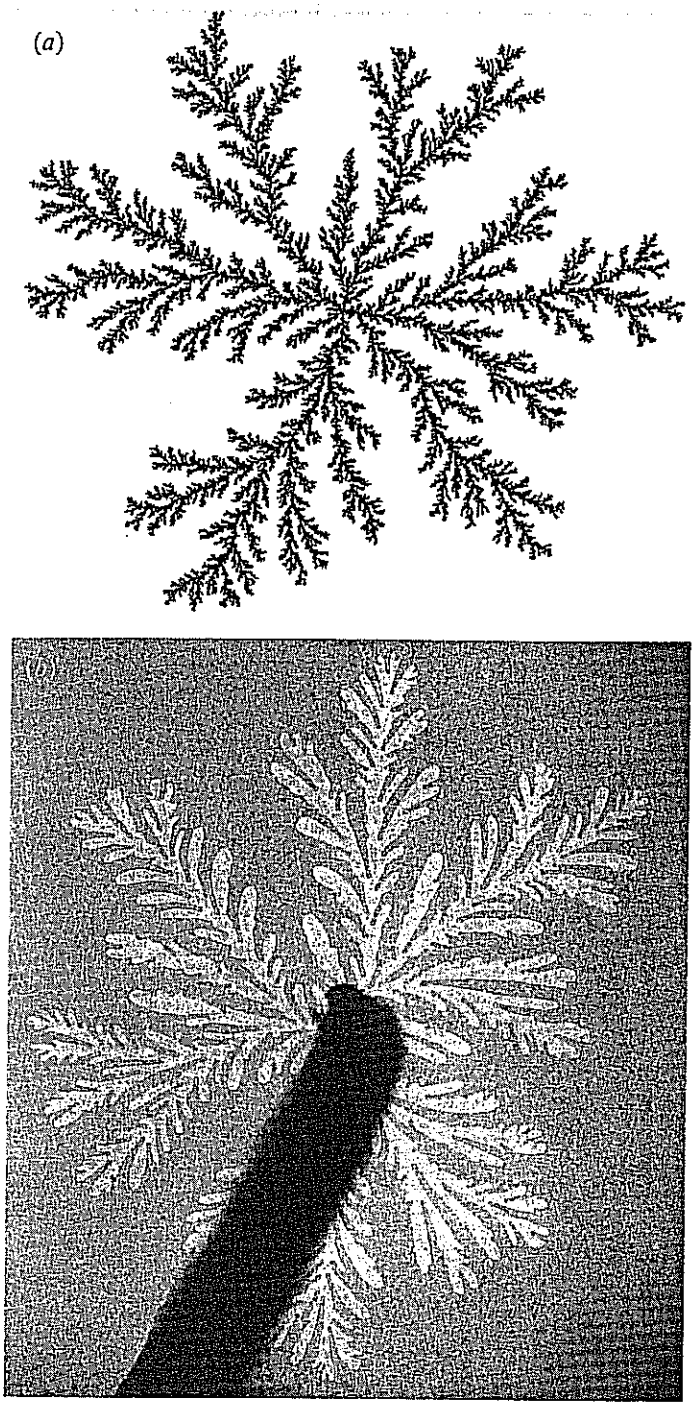

Figure 16. (*a*) An isotropic DLA grown off-lattice and having 10^6 particles (courtesy A. Arnéodo). (*b*) A radial fractal Saffman–Taylor fingering pattern.

In the following we will describe successively complex patterns obtained in isotropic and anisotropic situations. We will concentrate mainly on two of their characteristics.

(i) The scaling properties which give them a fractal character. Though understanding why patterns grown in a Laplacian field have a fractal structure is certainly a major problem, no complete theory exists about it yet.

(ii) The existence of a well-defined ensemble average for these fractal structures which, in a given geometry, is related to the corresponding stable solutions.

5.1 The isotropic case

5.1.1 Open growth: the fractal properties of DLA and viscous fingers

For some time the main issue in the field of complex patterns has been the measurement of their fractal dimension. The characterization of the fractal structures resulting from Laplacian growth was initially performed on radially grown DLA clusters (figure 16*a*) and several techniques were used. For DLA good scaling laws covering several decades were obtained. It was only later, after Paterson (1984) had pointed out the similarities of the equations of the two systems, that the fractal properties of viscous fingering were sought. This fractal structure was first observed in porous cells (Nittman, Daccord & Stanley 1985 and Chen *et al.* 1985) or with non-Newtonian fluids (Daccord, Nittmann & Stanley 1986; Lenormand, Touboul & Zarcone 1988 and Van Damme *et al.* 1988). It is more difficult to observe in the case of the pure Saffman–Taylor fingers (figure 16*b*). Several secondary effects can lead to spurious effects. Figure 16(*b*) is about the best that can be achieved; it was obtained in a small cell having a very thin spacing b, and oil with a very large viscosity. The applied pressures are high so that the glass plates have to be very thick (4 cm in figure 16*b*). If these conditions are met the growth is fractal and similar to DLA (Rauseo, Barnes & Maher 1987; Couder 1988; and May & Maher 1989). In spite of a limited range of scales between the large and the small scale the measured fractal dimension of the pattern shown in figure 16(*b*) is in good agreement with that of DLA.

The overall dynamics of fractal growth has received no general theoretical treatment as yet. At present it is only possible to describe the various processes at work in its built up. We can describe it in the geometry in which the linear stability analyses were performed, where an initial straight front separates two half-planes. As described above, the initial destabilization of

the front occurs at the characteristic small scale of the system. However, when the amplitude of the disturbances increases, the different protrusions of the front interact non-locally (as shown for DLA on figure 6), the fastest growing ones tending to screen off the others so that their growth is slowed down and ultimately stopped. Simultaneously these fastest protrusions have more space to grow so that they become unstable either by tip splitting or by side branching. The two opposing trends build up a fractal structure. The screening-off is responsible for the formation of larger and larger, increasingly widely spaced, trees (figure 6), a process often called coarsening. Simultaneously, tip splitting and side branching keep constantly generating the smaller scales of the fractal distribution.

5.1.2 *Confined growth: the ensemble-average properties*

We can now return to confined experimental configurations that limit the freedom of the system. The question we address concerns the structure of the very unstable patterns obtained when the two characteristic length scales of the problem are very different from each other but either fixed or controlled. This study concerns very unstable patterns obtained in the geometries in which stable smooth fronts have been found.

(i) The linear channel When fingers are grown in linear channels at large velocities (i.e. very small B, in the range from 10^{-4} to 10^{-6}) the fingers are strongly unstable (see figure 15*a*) with a large number of branches which have on average a width which scales on the capillary length at this velocity (Kopf-Sill & Homsy 1988 and Meiburg & Homsy 1988).

It can however be noted that on average a steady regime of growth is reached which needs to be characterized statistically (Arnéodo *et al.* 1989). For this purpose a large number N of identical runs of the same experiment can be performed at the same very small value of B so that N independent realizations of patterns of the type shown on figure 15(a) are obtained. If a transverse section of the cell is chosen and discretized it is possible to build up a histogram representing, for each point of the section, how many times during the N runs it has been occupied by air. A division by N gives the mean occupancy $r(y)$ in the transverse section. This function is zero on the two walls and maximum in the centre of the cell. It is a remarkable feature that the width λ' at mid-height of these histograms is 0.5, i.e. the same as that of the stable fingers.

This investigation can be pushed further by studying the analogous problem of the growth of DLA in a channel geometry (Arnéodo *et al.* 1989). A linear strip is used having a width W_s in units of the grid mesh size. The

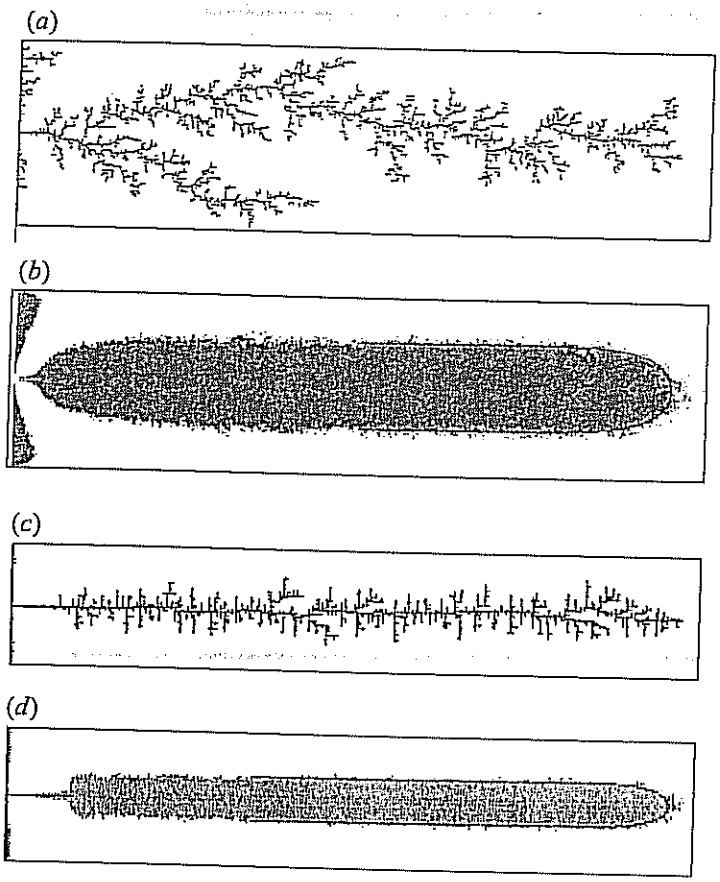

Figure 17. (*a*) A DLA grown in a strip of width $W = 128$ (Arnéodo *et al.* 1989). (*b*) The region of the channel with an occupancy rate above average in the strip in (*a*). (*c*) An anisotropic DLA grown in a strip of width $W = 64$. (*d*) The region of the channel with an occupancy rate above average in an anisotropic case.

system is confined by the lateral walls which reflect the randomly walking particles. The strip is open at one end and closed at the other. The particles stick onto the closed end of the strip. A large number of aggregates ($N = 512$) having the same total number M of particles are grown. One of them is shown on figure 17(*a*). For each point of the grid the number of realizations for which it has been occupied by a particle of an aggregate is counted. This number, divided by N, gives $\rho(x, y)$, the mean occupancy of this point.

The histogram of the occupancy along the axis of the linear strip shows that, except in the initial region and in the tip region, ρ is independent of x. This means that in the regions where the growth has ceased, the

cell's translational invariance imposes itself on the occupancy profile. In the transverse direction the occupancy profiles have a maximum value ρ_{max} at the centre ($y = 0$) and decrease to zero at the walls ($y = \pm W_s/2$). For viscous fingers, the profiles (a sharp step-shaped profile for stable fingers) become smoother with decreasing B, and the width of the regions which are never visited (along the walls) reduces. The profile of the histogram obtained for DLA far from the tip (in the region where the evolution is finished) is well fitted by

$$\rho(x, y) = \rho_{max}\cos^2(\pi y/W_s). \tag{5.2}$$

We obtain an average finger shape by seeking for each x the value y_m of y such that:

$$y_m = \frac{1}{\rho_{max}} \int_0^\infty \rho(x, y)\mathrm{d}y. \tag{5.3}$$

The important result is that the profile defined by $y_m(x)$ has (with some statistical fluctuation) the shape of Saffman–Taylor finger of width $\lambda = 0.5$ (figure 17*b*).

What relation is there between the fractal structure and the steady averages obtained here? When confined to the cell the mean growth has become translationaly invariant along the channel. Across the channel the patterns have retained their fractal character on all scales between W and l_u (or l_c). By varying either W (in the DLA experiments) or l_c (in the Saffman–Taylor experiments) it is found (Arnéodo *et al.* 1989 and 1996) that the maximum mean occupancy of the cell width varies as

$$\rho_{max} \propto (W_s/l_u)^{-0.33}. \tag{5.4}$$

It is a property of a fractal structure of dimension d_f that its section along a line has a dimension $d_f - 1$. This means that the resulting mean density along this line scales as $d_f - 2$. The experimental exponent -0.33 corresponds to $d_f = 1.67 \pm 0.01$, in agreement with the usual fractal dimension of DLA.

(ii) Sector-shaped cells A similar result is obtained in sector-shaped cells. Using the same procedures, unstable Saffman–Taylor fingers and DLA aggregates can be grown in wedges with angles θ_0. The relative angular width $\lambda_m(\theta_0)$ and the profile given by $y_m(x)$ can then be measured. Figure 11(*b*) shows that for all convergent cells and for weakly divergent ones, $\lambda_m(\theta_0)$ coincides remarkably well with the limiting width of the stable fingers obtained in these cells at small B. However, the mean profiles show a tendency to split and the envelope shape differs from that of the stable fingers (Levine & Tu 1992 and Arnéodo *et al.* 1996).

5.2 Non-isotropic case

Even though anisotropic patterns can be obtained with viscous fingering this is not the best system for the investigation of anisotropic fractal growth. This type of study is mostly done on anisotropic DLA or on dendrites.

5.2.1 Open growth: the fractal properties of anisotropic DLA and of dendrites

Preferential directions of growth can be given to diffusion-limited aggregates by several means. One is noise reduction, which reveals the anisotropy of the underlying lattice (Julien, Kolb & Botet 1984; Nittman & Stanley 1986; Meakin, Kertèsz & Vicsek 1986; Meakin 1987). The on-lattice procedure has a weak anisotropy, which is enhanced if the rules of the simulation are changed by requiring that a site should be visited m times before a particle sticks there. The larger the imposed m, the larger the effective anisotropy. Other rules permit the introduction of anisotropy in simulations performed without an underlying lattice (Eckmann *et al.* 1989). In both cases the resulting patterns (figure 18*a*) have the general aspect of dendrites and are very different from the usual DLA because tip splitting is inhibited. Only two processes are present here: screening which leads to coarsening; and side branching which keeps generating small-scale structures. In the simulations the fractal dimension decreases with increasing anisotropy. It is generally believed that, asymptotically, the very anisotropic clusters are self-affine fractals of dimension $d_f = 3/2$.

In order to obtain a comparable situation in crystal growth it is necessary to grow a single dendrite in a very thin cell (so as to have quasi-two-dimensionality). It is also necessary to be as close as possible to a Laplacian situation, i.e. have a very large diffusion length. In this limit the interaction between side branches is long range and similar to what it would be for a Laplacian field. A series of experiments on slowly growing dendrites was performed in a solution of ammonium bromide by Couder *et al.* (1990). Figure 18(*b*) is a photograph of such a dendrite. Though the crystal is compact along its axis, the competition between its side branches gives it the structure of a self-affine fractal. Far away from the tip the fractal dimension of this crystal is $d_f = 1.58 \pm 0.03$. Note that for faster growing crystals the structure is only fractal-like up to approximately the diffusion length scale l_D^c. At larger scales the morphology is still complex but the box-counting method shows that at those scales the fractal dimension becomes equal to 2. There is thus a transition to a dense branching morphology (Uwaha & Saito 1989).

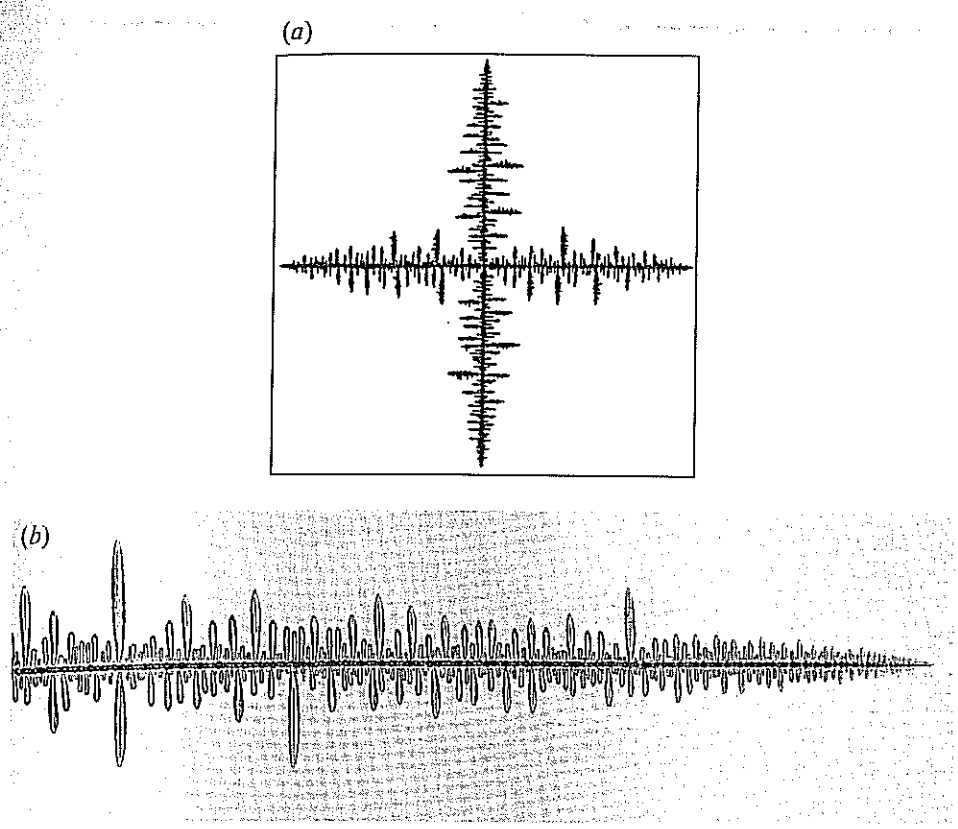

Figure 18. (*a*) An anisotropic DLA obtained with the noise-reduced technique with $m = 10$ (courtesy A. Arnéodo) (*b*) Photograph of a length of 1.25 mm of an ammonium bromide dendrite with a tip radius of curvature $r_d = 2.5\,\mu m$ (Couder *et al.* 1990).

5.2.2 *The ensemble-average properties*

(a) Anomalous viscous fingers and anisotropic DLA grown in a strip A generalization of the previous result about ensemble averages can be sought. (Couder *et al.* 1990; Arnéodo *et al.* 1991) in cells having plates engraved with a periodic square structure. It is also possible to grow anisotropic DLA patterns in a strip using the noise-reduced on-lattice simulation. Both in viscous fingering and in DLA when the easiest growth path is along the axis of the channel the unstable pattern is markedly narrower than for the isotropic case (figure 17*c*).

When the ensemble-averaging procedure is used again it produces transverse profiles which are narrower and sharper than in the isotropic case. For large m the value of ρ_{max} becomes independent of W_s. The regions of high occupancy are again in the shape of Saffman–Taylor fingers (figure 17*d*),

and analogous to the stable anomalous fingers. The profiles given by $y_m(x)$ are well fitted by Saffman–Taylor solutions, so the tip radius of curvature r_{ST}^f can be deduced from the observed λ. For a given m the mean profiles obtained in cells of different width W have different λ but the same r_{ST}^f. The radius of curvature is scaled on the lattice scale l_u, the coefficient of proportionality depending on the anisotropy (fixed by m):

$$r_{ST}^f = \alpha l_u. \tag{5.5}$$

This is precisely the characteristic of the selection of the stable anomalous Saffman–Taylor finger and of dendrites ((4.12) and (4.14)). Inspection of the patterns shows qualitatively that increasing m increases the anisotropy. There is an empirical relation (Arnéodo *et al.* 1991) between α and m: measurements of r_{ST}^f for m from 2 to 15 give $\alpha(m) \propto m^{-1.5}$. This relation is reminiscent of the power law of equation (4.12). Unfortunately the relation between m and the effective anisotropy is not known quantitatively.

The mean occupancy profile thus reflects the shape and the selection of the stable solution in both the isotropic and anisotropic cases. This correspondence can be pushed even one step further: Arnéodo *et al.* (1991) showed that there is a continuous transition in the fractal dimension from $d_f = 5/3$ to $d_f = 3/2$ when the anisotropy is increased and that this transition corresponds to the continous crossover between normal and anomalous fingers observed on figure 14.

(b) The dendrite For dendrites an average profile can also be defined (Couder *et al.* 1990) and this can be done on a single dendrite of the type shown on figure 18(*b*). The area $S(x)$ occupied by the two-dimensional pattern from the tip to a distance x along the axis is measured. A logarithmic plot of this area as a function of x shows a power law $S(x) \propto x^{1.5}$. This means that the area occupied by the dendrite is the same as that of a dense parabola. This virtual parabola has the same radius of curvature as the tip. In other words, the dendrite shown on figure 18 occupies, on average, the same area as if it had remained stable without any side branching. This property is apparent on one single realization because the stability of the tip creates a rate of occupancy $\rho_{\max} = 1$ along the axis of the dendrite (a situation also obtained in DLA for large m and in Saffman–Taylor fingering when the imposed anisotropy is large).

5.3 Mean-field theory

The first attempt at a mean-field theory for the mean occupation by fractal aggregates was due to Witten & Sander (1983). They proposed in the

continuum limit the equations

$$\frac{\partial \rho}{\partial t} = \nabla^2 w, \qquad \frac{\partial \rho}{\partial t} = w(\rho + l_u^2 \nabla^2 \rho), \tag{5.6}$$

in which ρ is the mean density of the aggregate, w the mean density of the randomly walking particles and l_u the lattice mesh size. The first equation is conservation of mass, the second represents the law that the DLA only grows when a site next to the existing aggregate is visited by a particle. V. Hakim showed that this set of equations could not be correct, as it leads, for the growth in a channel, to a density ρ decreasing as x^{-2}, and to the front going to infinity in a finite time. This effect is due to the absence, in the equation, of any lower threshold for the densities. In reality, because of the existence of the small scale, there is a finite threshold.

In order to take into account the existence of this threshold, Brenner, Levine & Tu (1991) suggested a heuristic modification in which the first term of the second equation is modified:

$$\frac{\partial \rho}{\partial t} = \nabla^2 w, \qquad \frac{\partial \rho}{\partial t} = w(\rho^\eta + l_u^2 \nabla^2 \rho), \tag{5.7}$$

the exponent being $\eta > 1$. This modification artificially introduces a cutoff in the growth rate. By numerical simulation Brenner *et al.* recovered the behaviour of the averages that were obtained numerically and experimentally and in particular the two selection mechanisms characteristic of the isotropic and anisotropic situations respectively. For the mean aggregates the Laplacian term can be written locally as $\partial^2/\partial n^2 + \kappa \partial/\partial n$ where $\boldsymbol{n}$ is the direction of the gradient and κ the local front curvature. As suggested by Brenner *et al.* this term, since it is curvature-dependent, can play a role similar to that of surface tension in the stable case. Further developments can be found in Levine & Tu (1992, 1993). However, in spite of the success of this set of equations, several problems remain, as pointed out by Arnéodo *et al.* (1996). There is no clear way to choose the cutoff parameter η introduced in (5.7). More fundamentally, the mean-field theory, in contradiction with reality, assumes the aggregate to be transparent to the diffusing particles.

6 Directional growth

Directional growth is not central to the present chapter, which is devoted to the morphogenetic aspects of viscous fingering, but we will discuss it briefly because of the interest in comparing it with free growth and also because it corresponds to several important industrial processes.

To each of the systems that have been examined here, it is possible to associate a variant in which the field P has a fixed imposed gradient. For viscous fingering, for instance, it corresponds to situations where a meniscus separating the fluid from air is located between two solid surfaces moving away from each other. Most such experiments model industrial processes in which viscous fluids are spread on solid surfaces. Experiments have been done between a plane and a cylinder (Pearson 1960; Savage 1977), between two co-rotating solid rollers (Pitts & Greiler 1961), and in the narrow passages of journal bearings (Taylor 1963). The same phenomenon occurs in the peeling of an adhesive tape (McEwan & Taylor 1966). In all these situations the space between the two solid surfaces forms a kind of Hele-Shaw cell, but of non-constant thickness. In the frame of reference of the boundaries, a low-viscosity fluid (i.e. air) is penetrating a high-viscosity fluid. The front is unstable to viscous fingering but the widening gap induces a pressure gradient that adds a stabilizing factor which has two effects. The fingering instability only appears above a finite instability threshold. Above this threshold the Saffman–Taylor instability is saturated by a nonlinear term so that a front is formed with fingers of finite and constant amplitude. These fingers leave behind them an uneven fluid layer so that in coating processes it is this unstability which limits the velocity at which fluids can be deposited on a solid surface.

From a theoretical point of view these coating instabilities are similar (Hakim *et al.* 1990) to directional solidification (in the limit of small Péclet number). In this latter type of experiment a liquid is pulled at constant velocity across a linear temperature gradient between two ovens at fixed temperatures. The temperatures are chosen so that the material solidifies in this gradient. In this situation the Mullins–Sekerka (1964) instability has a different dynamics (see Jackson & Hunt 1966; Langer 1980; Caroli *et al.* 1992 and references therein). There is now a return force towards a linear front fixed in the laboratory frame of reference. The crystallization front is stable at low velocities and only destabilizes above a critical pulling speed. It then forms a widely studied cellular pattern in which the cells have an amplitude limited by nonlinear terms. This instability is also of practical importance; it limits the pulling speed in the preparation of monocrystals.

Both of these instabilities generate linear fronts with a large number of identical cells. For this reason they have become model systems for the study of the nonlinear behaviour of extended one-dimensional systems. Some results in this area are summarized below.

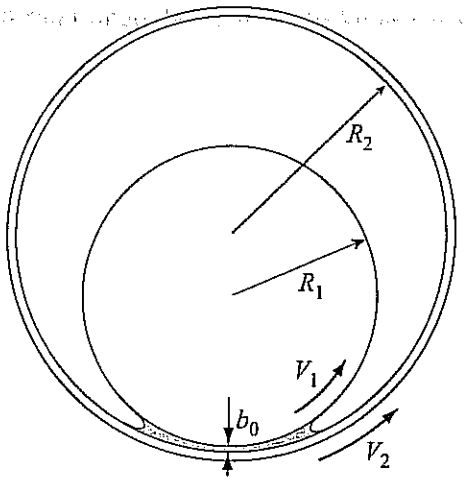

Figure 19. The printer's instability experimental set-up.

6.1 Isotropic case

From the point of view of nonlinear dynamics the directional viscous fingering experiment, having the widest variety of dynamical behaviours, is now known as 'the printer's instability' (Rabaud, Michalland & Couder 1990). It is composed of two horizontal cylinders of different radii (R_1 and R_2) placed one inside the other (figure 19). The inner cylinder has its axis parallel to the outer one, but off-centre so that at the bottom they are separated from each other by a small gap b_0 along one generatrix. A small amount of oil, sufficient to fill the gap, is introduced into the cell. A situation comparable to Saffman–Taylor fingering is obtained when the two cylinders are co-rotating so that the two walls have the same velocity in the gap region. The interesting meniscus here is located where the surfaces move away from each other. It remains stable up to a threshold value of the mean rotation. The instability appears as a supercritical process in which the front becomes a sinusoid of wavelength λ_c. As the velocities increase, the amplitude of the deformation grows and the front becomes a series of parallel fingers separated by thin oil walls (figure 20*a*). If the thickness gradient is weak the shape of these fingers is close to that of normal Saffman–Taylor fingers. The fundamental difference with the free growth is that the gradient limits the amplitude of these fingers and suppresses the long-range interaction responsible for the screening-off. A given finger has an amplitude limited by nonlinear terms and does not inhibit the growth of its neighbours anymore. In the case of a strict corotation of the two cylinders the pattern is not steady, but chaotic (figure 20*b*). Continuously some cells split and others are pinched off.

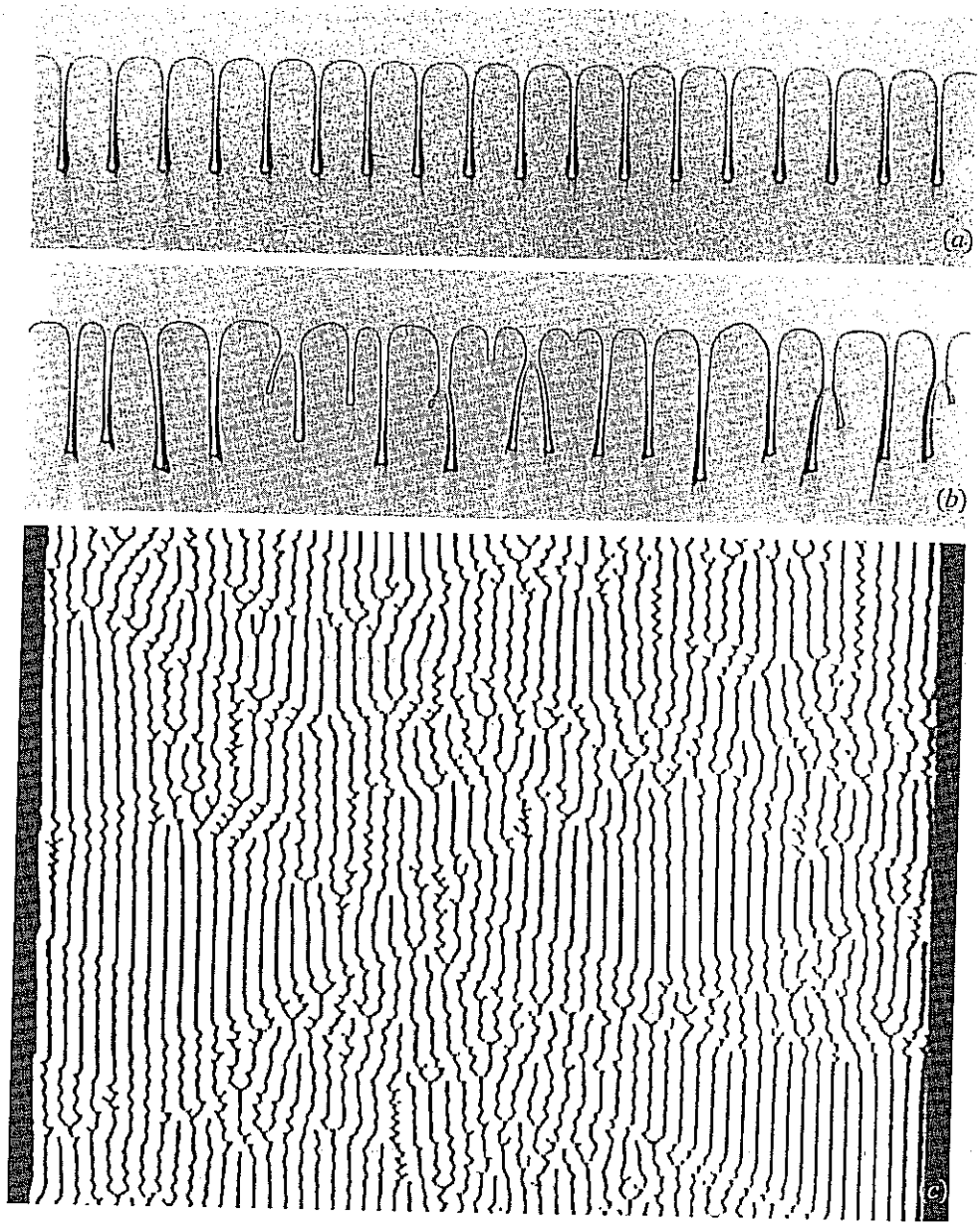

Figure 20. (*a*) Photograph of a detail of the cellular front of the printer's instability in a stable case ($\Omega_2 = 0$). (*b*) Photograph of a detail of a chaotic region of the cellular front. (*c*) Spatio–temporal evolution of the array of cells of the printer's instability in a regime of spatio–temporal intermittency. The time increases from the top to the bottom of the graph (Michalland *et al.* 1993).

The two cylinders can also be rotated with different tangential velocities V_1 and V_2. In the Saffman–Taylor fingering equivalent, this would imply that the two plates slide relative to each other in the direction of the finger motion, a situation never investigated. The nonlinear behaviour of the array of fingers, is that V_1 and V_2 form two independent control parameters. When only one of the cylinders is rotating the fingers are stable. When the second cylinder is set into co-rotation, temporal and spatial defects appear in the linear array of cells. As the co-rotation is increased, there is coexistence of chaotic domains (having constant formation and destruction of cells) with quiescent domains of steady, spatially periodic, cells. It is possible, by image processing, to reconstruct an image, each horizontal line of which gives the position, at a given time, of the walls separating the cells and where the evolution of these positions with time is displayed along the vertical axis (figure 20*c*). The two types of domain are clearly visible. The domains themselves are not stable: they appear, extend, then shrink and vanish and in their interplay they do not have symmetrical roles. The chaotic domains are active and emit waves which travel in the quiescent regions. When the waves travelling along the front reach a slightly disturbed region, a chaotic burst appears. So chaotic domains are related through space and time by the waves. For a given value of the control parameter the statistics of the sizes of the chaotic domains is steady. On increasing the second velocity the chaotic regions increase in size and ultimately the front becomes chaotic everywhere (Michalland, Rabaud & Couder 1993). The system thus becomes chaotic through spatio–temporal intermittency, a process characterized (Chaté & Maneville 1987) in the one-dimensional model phase equations introduced by Kuramoto & Tsuzuki (1976) and Sivashinsky (1985). In the experiment, as in the model, the transition to spatio-temporal chaos is similar to a second-order phase transition and exhibits critical exponents.

Finally, in the situation where the two surfaces move in opposite directions the front is still unstable, but through a subcritical bifurcation in which solitary waves are observed. Far from the threshold the front is formed entirely of left or right travelling cells separated by sources or sinks (Cummins, Fourtune & Rabaud 1993).

6.2 Anisotropic case

In the standard experiments on directional growth of crystals there is formation of a cellular front but it has a very different type of dynamics due to the preferential directions of growth imposed by the crystallographic anisotropy (Trivedi 1984). In most cases, as tip splitting is inhibited, the formation of

	Isotropic situation	Anisotropic situation
If the large and small scales are of the same order magnitude (e.g. $W > l_c$)	Stable curbed front with a width λ controlled by the large scale	Stable curved front with a tip having a radius of curvature controlled by the small scale
Dominant instability	Tip splitting	Side branching
If the large and small scales are very different (e.g. $W \gg l_c$)	Fractal structure with asymptotically $d_f = 5/3$. There exists a mean front with a width λ controlled by the large scale	Self-affine structure with asymptotically $d_f = 3/2$. There exists a mean front with a tip having a radius of curvature controlled by the small scale
Directional growth (two imposed scales of thesame order of magnitude)	Cellular front with spatio–temporal chaos	Cellular front with parallel dendrites

Table 1.

new cells is very difficult. As a result the front tends, at large velocities, to be formed of irregularly spaced dendritres. This behaviour is obtained in the printer's instability when parallel grooves are etched on one of the cylinders. In reverse, it is possible to eliminate the effect of anisotropy in directional solidification. This can be done by studying the phase transition of a liquid crystal (Flesselles, Simon & Libchaber 1991) or by making the front grow in a direction very far away from the axes of the crystal. In such cases a so-called seaweed morphology (Ihle & Müller Krumbaar 1994) is obtained which results from spatio–temporal chaos similar to that obtained in the printer's instability (Akamatsu, Faivre & Ihle 1995).

7 Conclusions

Several general conclusions can be drawn from this survey concerning Laplacian and diffusive growth patterns.

The growth in the inverse Stefan problem (as defined in § 1.1) is unstable. In the experimental or numerical reality there is always a lower limit on the size of the structures emerging from the growth. In the physical examples that we examined this small length scale could be obtained from the linear analysis of the stability of a plane front. Under this scale the front, stabilized by

surface tension, is smooth. The problems which have been solved are partial Stefan problems in which the growth occurs in cells with fixed boundaries. The successive steps are the following: when the existence of surface tension is neglected possible shapes of curved fronts can be found, depending on the geometry of the cell. In this limit, families of exact analytical solutions were found for two geometries: the linear cell and the sector-shaped cell. Then there is the problem of the selection. The results described above, which concern both stable curved fronts and ensemble-averaged fractal patterns, are summarized in table 1.

We have limited discussion here to Laplacian or quasi-Laplacian growth. In this area the main remaining question is that of a theory of fractal growth from first principles. As for other pattern forming systems, e.g. electrodeposition, dielectric breakdown, crack propagation etc., it is tempting to use analogies to analyse them. They are, however, complex and each of them requires a specific clarification of its physics before a valid use of analogies can be made.

A final question may be whether some biological morphogenetic processes, such as, for example, the formation of the venous system, are related to the type of growth pattern we have examined. In other words, in the living world do these physical processes contribute to the generation of forms? Such questions, in the style of D'Arcy Thompson, remain open.

References

Akamatsu, S., Faivre, G. & Ihle, T. 1995 Symmetry-broken double fingers and seaweed patterns in thin film directional solidification of a nonfaceted cubic crystal. *Phys. Rev.* E **51**, 4751–4773.

Arnéodo, F. Argoul, A., Couder, Y. & Rabaud, M. 1991 Anisotropic Laplacian growth: from diffusion-limited aggregates to dendritic fractals. *Phys. Rev. Lett.* **66**, 2332–2335.

Arnéodo, A., Couder, Y., Grasseau, G., Hakim, V. & Rabaud, M. 1989 Uncovering the analytical Saffman–Taylor finger in unstable viscous fingering and diffusion-limited aggregation. *Phys. Rev. Lett.* **63**, 984–987.

Arnéodo, A., Elezgaray, J., Tabard M. & Tallet, F. 1996 Statistical analysis of off-lattice diffusion-limited aggregates in channel and sector geometries. *Phys Rev.* E **53**, 6200–6223.

Bataille, J. 1968 Stabilité d'un déplacement radial non-miscible. *Revue Inst. Pétrole* **23**, 1349–1364.

Ben Amar, M. 1990 Dendritic growth at arbitrary undercooling. *Phys. Rev.* A **41**, 2080–2092.

Ben Amar, M. 1991*a* Exact self-similar shapes in viscous fingering. *Phys. Rev.* A **43**, 5724–5727.

Ben Amar, M. 1991*b* Viscous fingering in a wedge. *Phys. Rev.* A **44**, 3673–3685.

BEN AMAR, M., HAKIM, V., MASHAAL, M. & COUDER, Y. 1991 Self-dilating fingers in wedge shaped Hele-Shaw cells. *Phys. Fluids* A **3**, 2039–2042.

BEN JACOB, E., GODBEY, R., GOLDENFELD, N. D., KOPLIK, J., LEVINE, H., MUELLER, T. & SANDER, L. M. 1985 Experimental demonstration of the role of anisotropy in interfacial pattern formation. *Phys. Rev. Lett.* **55**, 1315–1318.

BEN JACOB, E., SCHMUELI, H., SHOCHET, O. & TENENBAUM, A. 1992 Adaptative self-organisation during growth of bacterial colonies. *Physica* A **187**, 378–424.

BENSIMON, D., KADANOFF, L. P., LIANG, S., SHRAIMAN, B. I. & TANG, C. 1986*a* Viscous flow in two dimensions. *Rev. Mod. Phys.* **58**, 977–999.

BENSIMON, D. & PELCÉ, P. 1986*b* Tip splitting solutions to a Stefan problem. *Phys. Rev.* A **33**, 4477–4478.

BENSIMON, D., PELCÉ, P. & SHRAIMAN, B. I. 1987 Dynamics of curved fronts and pattern selection. *J. Phys. Paris* **48**, 2081–2087.

BOUISSOU, P., CHIFFAUDEL, A., PERRIN, B. & TABELING, P. 1990 Dendritic side branching forced by an external flow. *Europhys. Lett.* **13**, 89–94.

BRENNER, E., LEVINE, H. & TU, Y. 1991 Mean field theory for the diffusion-limited aggregation in low dimensions. *Phys. Rev. Lett.* **66**, 1978–1981.

BRETHERTON, F. P. 1961 The motion of long bubbles in tubes. *J. Fluid Mech.* **10**, 166–188.

BUKA, A., KERTESZ, A. J. & VICSEK, T. 1986 Transitions of viscous fingering patterns in nematic liquid crystals *Nature* **323**, 424–425.

CAROLI, B., CAROLI, C., MISBAH, C. & ROULET, B. 1987 On velocity selection for needle crystals in fully non-local model of solidification *J. Phys. Paris* **48**, 547–552.

CAROLI, B., CAROLI, C. & ROULET, B. 1987 On the linear stability of needle crystals: evolution of a Zel'dovich localised front deformation. *J. Phys.* **48**, 1423–1437.

CAROLI, B., CAROLI, C. & ROULET, B. 1992 Instabilities of planar solidification fronts. In *Solids Far From Equilibrium* (ed. C. Godrèche). Cambridge University Press.

CHATÉ, H. & MANEVILLE, P. 1987 Transition to turbulence via spatiotemporal intermittency. *Phys. Rev. Lett.* **58**, 112–115.

CHEN, JING-DEN & WILKINSON, D. 1985 Pore scale viscous fingering in porous media. *Phys. Rev. Lett.* **55**, 1892–1818.

CHUOKE, R. L., VAN MEURS, P. & VAN DER POL, C. 1959 The instability of slow immiscible viscous liquid-liquid displacements in permeable media. *Petrol. Trans. AIME* **216**, 188–194.

COMBESCOT, R. & BEN AMAR, M. 1991 Selection of Saffman–Taylor fingers in the sector geometry. *Phys. Rev. Lett.* **67**, 453–456.

COMBESCOT, R. & DOMBRE, T. 1989 Selection in the anomalous Saffman–Taylor fingers induced by a bubble. *Phys. Rev.* A **39**, 3525–3535.

COMBESCOT, R., DOMBRE, T., HAKIM, V., POMEAU, Y. & PUMIR, A. 1986 Shape selection of Saffman–Taylor fingers. *Phys. Rev. Lett.* **56**, 2036–2039.

COMBESCOT, R., DOMBRE, T., HAKIM, V., POMEAU, Y. & PUMIR, A. 1988 Analytic theory of the Saffman–Taylor fingers. *Phys. Rev.* A **37**, 1270–1283.

COUDER, Y., CARDOSO, O., DUPUY, D., TAVERNIER, P. & THOMÉ, H. 1986*a* Dendritic growth in the Saffman–Taylor experiment. *Europhys. Lett.* **2**, 437–443.

COUDER, Y. GERARD, N. & RABAUD, M. 1986*b* Narrow fingers in the Saffman–Taylor instability. *Phys. Rev.* A **34**, 5175–5178.

COUDER, Y. 1988 Viscous fingering in a circular geometry. In *Random Fluctuations and Pattern Growth* (ed. H. E. Stanley & N. Ostrowsky). Kluwer.

COUDER, Y., ARGOUL, F., ARNÉODO, A., MAURER, J. & RABAUD, M. 1990 Statistical

Properties of fractal dendrites and anisotropic diffusion-limited aggregates. *Phys. Rev.* A **42**, 3499–3503.

COUDER, Y. 1991 Growth Patterns: from the stable curved fronts to fractal structures. In *Chaos, Order and Patterns* (ed. R. Artuso, P. Cvitanovic & G. Casati). Plenum.

CUMMINS, H. Z., FOURTUNE L. & RABAUD, M. 1993 Successive bifurcations in directional viscous fingering. *Phys. Rev.* E **47**, 1727–1738.

D'ARCY THOMPSON, W. 1917 *On Growth and Form*, vols. 1 and 2. Cambridge University Press (reissued in 1952).

DACCORD, G., NITTMANN J. & STANLEY, H. E. 1986 Radial viscous fingers and diffusion-limited aggregation fractal dimension and growth sites. *Phys. Rev. Lett.* **56**, 336–339.

DORSEY, A. T. & MARTIN, O. 1987 Saffman–Taylor fingers with anisotropic surface tension. *Phys. Rev.* A **35**, 3989–3992.

DOUGHERTY, A. & GOLLUB, J. P. 1988 Steady state dendritic growth in NH_4Br from solution. *Phys. Rev.* A **38**, 3043–3053.

ECKMANN, J. P., MEAKIN, P., PROCACCIA, I. & ZEITAK, R. 1989 Growth and form of noise reduced diffusion-limited aggregation. *Phys. Rev.* A **29**, 3185–3195.

FLESSELES, J. M., SIMON, A. J. & LIBCHABER, A. J. 1991 Dynamics of one-dimensional interfaces: an experimentalist's view. *Adv. Phys.* **40**, 1–51.

FUKIKAWA, H. & MATSUSHITA, M. 1991 Bacterial fractal growth in the concentration field of nutrient. *J. Phys. Soc. Japan* **60**, 88–94.

HAKIM, V., RABAUD, M., THOMÉ, H. & COUDER, Y. 1990 Directional growth in viscous fingering. In *New Trends in Nonlinear Dynamics and Pattern Forming Phenomena* (ed. by P. Coullet & P. Huerre). Plenum.

HOMSY, G. M. 1987 Viscous fingering in porous media. *Ann. Rev. Fluid Mech.* **19**, 271.

HONG, D. C. & LANGER, J. S. 1986 Analytical theory of the selection mechanism in the Saffman–Taylor problem. *Phys. Rev. Lett.* **56**, 2032–2035.

HONG, D. C. & LANGER, J. S. 1987 Pattern selection and tip perturbation in the Saffman–Taylor problem. *Phys. Rev.* A **36**, 2325–2332.

HONJO, H., OHTA, S. & MATSUSHITA, M. 1986 Irregular fractal like crystal growth of ammonium chloride. *J. Phys. Soc. Japan* **55**, 2487–2490.

HOWISON, S. D. 1986 Fingering in Hele-Shaw cells, *J. Fluid Mech.* **167**, 439–453.

HUANG, S. C. & GLICKSMAN, M. E. 1982 Fundamentals of dendritic solidification I. Steady-state tip growth. *Acta Metall.* **29**, 701–715; II. Development of sidebranch structure. *Acta Metall.* **29**, 717–734.

HULL, D. 1999 *Fractology*, Cambridge University Press.

IHLE, T. & MÜLLER KRUMBAAR, H. 1994 Fractal and compact growth morphologies in phase transitions with diffusion transport. *Phys. Rev.* E **49**, 2972–2991.

IVANTSOV, G. P. 1947 Temperature field around spherical, cylindrical and acicular crystal growing in a supercooled melt. Translated from *Dokl. Acad. Nauk.* **58**(4), 567–569.

JACKSON, K. A. & HUNT, J. D. 1966 Transparent compounds that freeze like metals. *Trans. Metal. Soc. AIME* **236**, 1129–1215.

JULIEN, R., KOLB, M. & BOTET, M. 1984 Diffusion limited aggregation with directed and anisotropic diffusion. *J. Phys. Paris* **45**, 395–399.

KADANOFF, L. P. 1985 Simulating hydrodynamics: a pedestrian model. *J. Statist. Phys.* **39**, 267–283.

KESSLER, D., KOPLIK, J. & LEVINE, H. 1986*a* Steady-state dendritic crystal growth. *Phys. Rev.* A **33**, 3352–3357.

KESSLER, D., KOPLIK, J. & LEVINE, H. 1986*b*. Dendritic growth in a channel. *Phys. Rev.* A **34**, 4980–4987.

KESSLER, D., KOPLIK, J. & LEVINE, H. 1988 Pattern selection in fingered growth phenomena. *Adv. Phys.* **37**, 255–339.

KESSLER, D. & LEVINE, H. 1987 Determining the wavelength of dendritic side-branches. *Europhys. Lett.* **4**, 215–221.

KOPF-SILL A. & HOMSY, G. M. 1987 Narrow fingers in Hele-Shaw cells. *Phys. Fluids* **30**, 2607–2609.

KOPF-SILL, A. R. & HOMSY, G. M. 1988 Nonlinear unstable viscous fingers in Hele-Shaw flows, I Experiments. *Phys. Fluids* **31**, 242–249.

KURAMOTO, Y. & TSUZUKI, T. 1976 Persistent propagation of concentration waves. *Prog. Theor. Phys.* **55**, 356–369.

LANDAU, L. & LEVICH, B. 1942 Dragging of a liquid by a moving plate. *Acta Physico-chimica URSS* **17**, 42–54.

LANGER, J. S. 1980 Instabilities and pattern formation in crystal growth. *Rev. Mod. Phys.* **52**, 1–28.

LANGER, J. S. 1987 Lectures in the theory of pattern formation. In *Chance and Matter* (ed. J. Souletie, J. Vannimenus & R. Stora). North-Holland.

LENORMAND, R., TOUBOUL, E. & ZARCONE, C. 1988 Numerical models and experiments on immiscible displacements in porous media. *J. Fluid Mech.* **189**, 165–187.

LEVINE, H. & TU, Y. 1992 Mean field diffusion-limited aggregation in radial geometries. *Phys. Rev.* A **45**, 1053–1057.

LEVINE, H. & TU, Y. 1993 Theory of diffusion-limited growth. *Phys. Rev.* E **48**, R 4207–4210.

LIANG, S. 1986 Random walk simulations of flow in Hele-Shaw cells. *Phys. Rev.* A **33**, 2663–2674.

MCCLOUD, K. V. & MAHER, J. V. 1995 Experimental perturbations to Saffman Taylor flow. *Phys. Rep.* **260**, 139–185.

MCEWAN, A. D. & TAYLOR, G. I. 1966 The peeling of a flexible strip attached by a viscous adhesive. *J. Fluid Mech.* **26**, 1–15.

MCLEAN, J. W. & SAFFMAN, P. G. 1981 The effect of surface tension on the shape of fingers in a Hele-Shaw cell. *J. Fluid Mech.* **102**, 455–469.

MANDELBROT, B. B. 1982 *The Fractal Geometry of Nature*. Freeman, San Francisco.

MAURER, J., PERRIN, B. & TABELING, P. 1991 Three-dimensional structures of NH_4Br dentrites growing in a gel. *Europhys. Lett.* **14**, 575–579.

MAY, S. E. & MAHER, J. V. 1989 Fractal dimension of radial fingering patterns. *Phys. Rev.* A **40**, 1723–1726.

MEAKIN, P. 1987 Noise reduced diffusion-limited aggregation. *Phys. Rev.* A **36**, 332–339.

MEAKIN, P., KERTESZ, J. & VICZEK, T. 1988 Noise reduced diffusion-limited deposition. *J. Phys.* A **21**, 1271–1281.

MEIBURG, R. & HOMSY, G. M. 1988 Nonlinear unstable viscous fingers in Hele-Shaw flows, II Numerical simulations. *Phys. Fluids* **31**, 429–439.

MICHALLAND, S., RABAUD, M. & COUDER, Y. 1993 Transition to chaos by spatio-temporal intermittency in directional viscous fingering. *Europhys. Lett.* **22**, 17–22.

MULLINS, W. W. & SEKERKA, R. F. 1964 Stability of a planar interface during solidification of a dilute binary alloy. *J. Appl. Phys.* **35**, 444–451.

MUTHUKUMAR, M. 1983 Mean field theory for diffusion-limited cluster formation. *Phys. Rev. Lett.* **50**, 839–842.

NITTMANN, J., DACCORD, G. & STANLEY, H. E. 1985 Fractal growth of viscous fingers: quantitative characterization of a fluid instability phenomenon. *Nature* **314**, 141–144.

NITTMANN, J. & STANLEY, H. E. 1986 Tip splitting without interfacial tension and dendritic growth patterns arising from molecular anisotropy. *Nature* **321**, 663–668.

PATERSON, L. 1981 Radial viscous fingering in a Hele-Shaw cell. *J. Fluid Mech.* **113**, 513–529.

PATERSON, L. 1984 Diffusion limited aggregation and two-fluid displacements in porous media. *Phys. Rev. Lett.* **52**, 1621–1623.

PATERSON, L. 1985 Fingering with miscible fluids in a Hele-Shaw cell. *Phys. Fluids* **28**, 26–30.

PEARSON, J. R. A. 1960 The instability of uniform viscous flow under rollers and spreaders. *J. Fluid Mech.* **7**, 481–500.

PELCÉ, P. 1988 *Dynamics of Curved Fronts.* Academic.

PELCÉ, P. & CLAVIN, P. 1987 The stability of curved fronts. *Europhys. Lett.* **3**, 907–913.

PITTS, E. & GREILLER, J. 1961 The flow of thin films between rollers. *J. Fluid Mech.* **11**, 33–50.

PO ZEN WONG 1999 *Methods on the Physics of Porous Media.* Academic.

POMEAU, Y. & BEN AMAR, M. 1992 Dendritic growth and related topics. In *Solids Far From Equilibrium* (ed. C. Godrèche). Cambridge University Press.

QUIAN, X. W. & CUMMINS, H. Z. 1990 Dendritic sidebranching initiation by a localized heat pulse. *Phys. Rev. Lett.* **64**, 3038–3041.

RABAUD, M., COUDER, Y. & GERARD, N. 1988 The dynamics and stability of anomalous Saffman–Taylor fingers. *Phys. Rev.* A **37**, 935–947.

RABAUD, M., MICHALLAND, S. & COUDER, Y. 1990 Dynamical regimes of directional viscous fingering: spatio-temporal chaos and wave propagation. *Phys. Rev. Lett.* **64**, 184–187.

RAUSEO, S. N., BARNES, P. D. & MAHER J. V. 1987 Development of radial fingering patterns. *Phys. Rev.* A **35**, 1245–1251.

REINELT, D. A. 1987 The effect of thin film variations and transverse curvature on the shape of fingers in a Hele-Shaw cell. *Phys. Fluids* **30**, 2617–2623.

SAFFMAN, P. G. 1986 Viscous fingering in Hele-Shaw cells, *J. Fluid Mech.* **173**, 73–94.

SAFFMAN, P. G. & TAYLOR, G. I. 1958 The penetration of a fluid into a porous medium or Hele-Shaw cell containing a more viscous fluid. *Proc. R. Soc. Lond.* A **245**, 312–329.

SANDER, L. M., RAMANLAL P. & BEN JACOB, E. 1985 Diffusion-limited aggregation as a deterministic growth process. *Phys. Rev.* A **32**, 3160–3163.

SARKAR, S. K. 1985 Saffman–Taylor intability and pattern formation in diffusion-limited aggregation. *Phys. Rev.* A **32**, 3114–3116.

SARKAR, S. K. & JASNOW, D. 1989 Viscous fingering in an anisotropic Hele-Shaw cell. *Phys. Rev.* A **39**, 5299–5307.

SAVAGE, M. D. 1977 Cavitation in lubrication. Part 1. On boundary conditions and cavity-fluid interfaces. *J. Fluid Mech.* **80**, 743–755.

SCHWARTZ, L. & DEGREGORIA, A. 1987 Simulations of Hele-Shaw fingering with finite capillary number effect included. *Phys. Rev.* A **35**, 276–279.

SHRAIMAN, B. 1986 Velocity selection in the Saffman–Taylor problem. *Phys. Rev. Lett.* **56**, 2028–2031.

SHRAIMAN B. & BENSIMON, D. 1984 Singularities in non-local interface dynamics. *Phys. Rev.* A **30**, 2840–2842.
SIVACHINSKY, G. I. 1985 Weak turbulence in periodic flows. *Physica* D **17**, 243–255.
TABELING, P., ZOCCHI, G. & LIBCHABER, A. 1987 An experimental study of the Saffman–Taylor instability. *J. Fluid Mech.* **177**, 67–82.
TANVEER, S. 1987*a* Analytic theory for the selection of a symmetric Saffman–Taylor finger in a Hele-Shaw cell. *Phys. Fluids* **30**, 1589–1605.
TANVEER, S. 1987*b* Analytic theory of the linear stability of the Saffman–Taylor finger. *Phys. Fluids* **30**, 2318–2329.
TANVEER, S. 1990 Analytic theory for the selection of Saffman–Taylor fingers in the presence of thin film effects. *Proc. R. Soc. Lond.* A **428**, 511–545.
TANVEER, S. 1991 Viscous displacement in a Hele-Shaw cell. In *Asymptotics Beyond all Orders* (ed. H. Segur, S. Tanveer & H. Levine), p. 131. Plenum.
TAYLOR, G. I. 1963 Cavitation of a viscous fluid in narrow passages. *J. Fluid Mech.* **16** 595–619.
THOMÉ, H., RABAUD, M., HAKIM V. & COUDER, Y. 1989 The Saffman–Taylor instability: from the linear to the circular geometry. *Phys. Fluids* A **1**, 224–240.
THOMÉ, H., COMBESCOT, R. & COUDER, Y. 1990 Controlling singularities in the complex plane: experiments in real space. *Phys. Rev.* A **41**, 5739–5742.
TOKUYAMA, M. & KAWASAKI, K. 1984 Fractal dimension for diffusion-limited aggregates. *Phys. Lett.* **100A**, 337–340.
TRIVEDI, R. 1984 Interdendritic spacing, Parts I and II *Metall. Trans.* A **15**, 977–982.
UWAHA, M. & SAITO, Y. 1989 Aggregation growth in a gas of finite density: velocity selection via fractal dimension of diffusion-limited aggregation. *Phys. Rev.* A **40**, 4716–4723.
VAN DAMME, H., ALSAC, E., LAROCHE, C. & GATINEAU, L. 1988 On the relative roles of low surface tension and non-newtonian rheological properties in fractal fingering. *Europhys. Lett.* **5**, 25–30.
VANDEN BROECK, J. M. 1983 Fingers in a Hele-Shaw cell with surface tension. *Phys. Fluids* **26**, 2033–2034.
VICSEK, T. 1984 Pattern formation in diffusion-limited aggregation. *Phys. Rev. Lett.* **53**, 2281–2284.
VICSEK, T. 1989 *Fractal Growth Phenomena*. World Scientific.
WITTEN, T. & SANDER, L. M. 1981 Diffusion-limited aggregation, a kinetic critical phenomenon. *Phys. Rev. Lett.* **47**, 1400–1403.
WITTEN, T. & SANDER, L. M. 1983 Diffusion-limited aggregation. *Phys. Rev.* B **27**, 5686–5697.
ZEL'DOVICH, YA. B., ISTRATOV, A. G., KIDIN, N. I. & LIBROVICH, V. B. 1980 Flame propagation in tubes: hydrodynamics and stability. *Combust. Science Technol.* **24**, 1–13.
ZOCCHI, G., SHAW, B. E., LIBCHABER, A. & KADANOFF, L. P. 1987 Finger narrowing under local perturbations in the Saffman–Taylor problem. *Phys. Rev.* A **36**, 1894–1900.